Title	Electrostatic Properties of Organic/Insulator and Organic/Organic Interfaces Studied by Kelvin Probe Force Microscopy
Author(s)	Mishima, Ryota
Citation	大阪大学, 2012, 博士論文
Version Type	VoR
URL	https://hdl.handle.net/11094/26846
rights	
Note	

Electrostatic Properties of Organic/Insulator and Organic/Organic Interfaces Studied by Kelvin Probe Force Microscopy

RYOTA MISHIMA

MARCH 2012

Electrostatic Properties of Organic/Insulator and Organic/Organic Interfaces Studied by Kelvin Probe Force Microscopy

A dissertation submitted to
THE GRADUATE SCHOOL OF ENGINEERING SCIENCE
OSAKA UNIVERSITY
in partial fulfillment of the requirements for the degree of
DOCTOR OF PHILOSOPHY IN SCIENCE

BY

RYOTA MISHIMA

MARCH 2012

論文内容の要旨

〔題　名〕 Electrostatic Properties of Organic/Insulator and Organic/Organic Interfaces Studied by Kelvin Probe Force Microscopy (ケルビンプローブフォース顕微鏡を用いた有機／絶縁体および有機／有機界面の静電的性質の研究)

学位申請者　三島良太

真空準位のシフトは異種物質界面の静電気的な性質を示す重要な要素の一つである。無機物質界面で電荷移動が真空準位のシフトの主たる起源とされており、有機分子を含む界面でも電荷移動を用いて解釈する流れにある。しかし、電子的な相関の少ない有機／絶縁体および有機／有機界面にまで適用できるかは不明瞭なままである。本論文では、ケルビンプローブフォース顕微鏡を用いて、Si酸化膜上に成長させたπ共役系分子の単分子膜と単分子ヘテロ接合膜の界面における真空準位のシフトを測定し、それぞれの静電的な性質について研究した。

有機／絶縁体の研究では、表面の電子状態と電荷状態を制御するためシラン分子を修飾した酸化膜を用い、その上に成長させた単分子膜の真空準位のシフトを測定した。真空準位のシフトは酸化膜表面の電子状態ではなく電荷分布に依存することがわかった。これは分子と基板の間で電荷移動が起こらず、表面電荷によって誘起された分子内の分極が真空準位のシフトの主たる起源であることを示す。さらに、アルキル鎖を付加させた分子を用いると表面電荷の効果は緩和され分子構造の非対称性に由来する真空準位のシフトが得られることがわかった。

有機／有機界面の研究では、π平面が向かい合うface-to-face構造と縦に並ぶhead-to-tail構造をもった単分子ヘテロ接合膜を作製し、界面の構造と真空準位のシフトの関係について議論した。face-to-face構造では電荷移動に基づく真空準位のシフトが得られ、head-to-tail接合ではそれぞれの分子内に分極が生じていることがわかった。これは真空準位のシフトが分子のπ軌道の位置関係に強く依存することを示す。これまで電荷移動が重要視されたのはヘテロ接合膜内に異なる吸着構造が混在し、平均化された結果が測定されていたためだと考えられる。本研究では有機／有機界面の構造制御に成功したため、π軌道の混成に基づく真空準位のシフトを得たといえる。

Contents

1. Introductions

2. Basic Principle of Kelvin Probe Force Microscopy

3. Experimental Setup

4. Electrostatic Properties of Organic-Insulator interfaces

5. Geometric Dependence of Electrostatic Properties at Donor-Acceptor Interfaces

Chapter 1

Introductions

1-1. Organic Electronics

In the last two decades, enormous research efforts have been directed towards electronic devices based on organic materials (OMs), such as organic field-effect transistors (OFETs), organic light-emitting diodes (OLEDs), and organic photovoltaic cells (OPVCs). It has been demonstrated that the performance of organic devices is strongly governed by the properties of organic-metal (O-M), organic-insulator (O-I), and organic-organic (O-O) interfaces. The properties of an O-M interface determine the carrier injection characteristics in organic electronic devices. Thin insulating films tune the electronic structure of an underlying metallic electrode, leading to control of the carrier injection into OMs. The energy level alignment of an O-I interface affects the carrier transport properties. The properties of an O-O interface correlate with hole-electron recombination and dissociation. Therefore, great effort has been exerted to clarify the electronic and geometric structures of the interfaces in order to improve device performance.

This thesis focuses on the properties of plate-like grown on insulators. It is known that plate-like molecules are the most promising for applications because of their high mobility, ease of chemical modification, and well-defined layer growth (Fig. 1-1(a)).

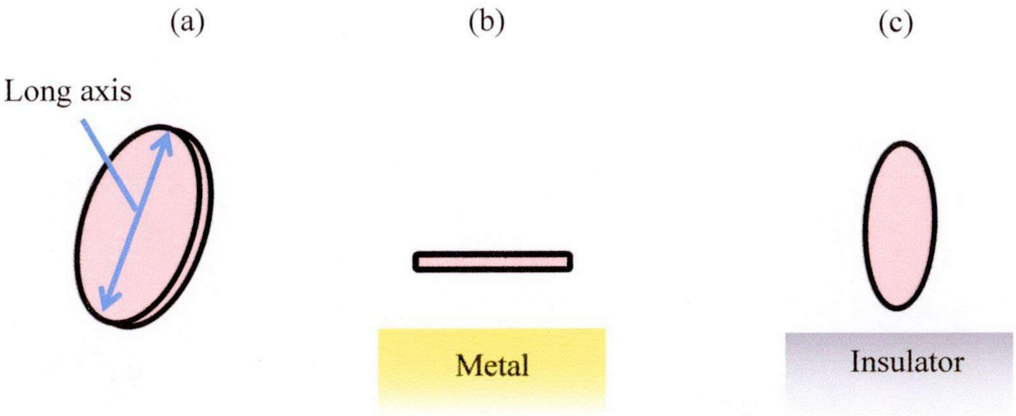

Figure 1-1. (a) An illustration of a plate-like molecule. Molecular orientations in organic films on (b) metal and (c) insulator substrates.

1-2. Organic-Metal Interfaces

The geometric and electronic properties at an O-M interface are well documented both experimentally and theoretically [2-7]. The geometric properties are characterized by the relation between intermolecular and organic-substrate interactions. Usually, a plate-like molecule stays on a metal substrate with intermolecular plane parallel to the surface (Fig. 1-1(b)) since a molecule-substrate interaction is stronger than an intermolecular interaction.

One of the most useful and important concepts to describe the interfacial electronic structures is the "vacuum level (VL) shift" at O-M interfaces. A VL shift have been measured by Photoemission Spectroscopy (PS) and Kelvin Probe Force Microscopy (KPFM). Seki [1] and Kahn [2] have shown that the energy diagram at an O-M interface is described not by the Mott-Schottky model but by the VL shift model resulting from the formation of an interfacial double layer. Many studies on the origin of this double layer have been reported. The charge transfer as well as the push-back effect are the essential factors for the VL shift of molecules on metal substrates [2-7].

One of widely accepted theoretical approaches for determining the VL shift at an O-M interface is an Induced Density of Interfacial States (IDIS) model. The IDIS model was established to explain the charge transfer at the interface between an inorganic semiconductor and a metal [8-10]. Kahn's group introduced the IDIS model to explain the energy level alignment at the O-M interface [11,12]. In this model, a charge neutrality level (CNL) is used as the quasi-Fermi level which behaves as a semiempirical surface (interface) state located in the bandgap (Fig. 1-2(a)). When a metal and a molecule are brought into contact, the Fermi level of the metal tends to align with a CNL of the molecule as a result of charge transfer (Fig. 1-2(b)). A resulting work function for an O-M interface ($\Phi_{\mathrm{org/metal}}$) and a VL shift ($\Delta$) are given by

$$\Phi_{\mathrm{org/metal}} - \mathrm{CNL} = S(\Phi_{\mathrm{metal}} - \mathrm{CNL}), \tag{1-1}$$

$$\Delta = (1 - S)(\Phi_{\mathrm{metal}} - \mathrm{CNL}), \text{ and} \tag{1-2}$$

$$S = d\Phi_{\mathrm{org/metal}}/d\Phi_{\mathrm{metal}}. \tag{1-3}$$

VL shifts at an O-M interface are often described as linear functions of work function of substrates by using these equations. Slope of these functions is called the slope parameter (S) of OMs.

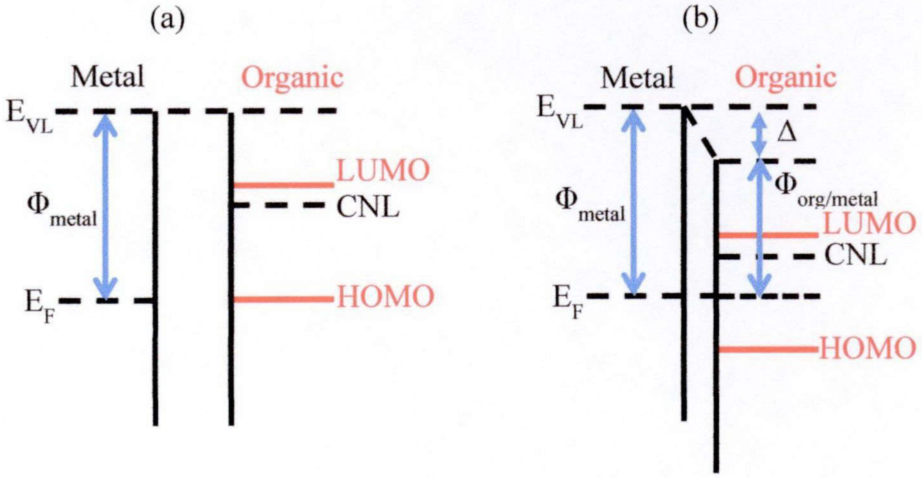

Figure 1-2. Energy diagrams (a) in separation of OM with metal and (b) after contact of them. The highest occupied molecular orbital and the lowest unoccupied molecular orbital are described as HOMO and LUMO, respectively.

1-3. Organic-Insulator Interfaces

The geometric properties at an O-I interface have been studied by X-ray diffraction techniques. Plate-like OMs orient on an insulator substrate with their long axes perpendicular to the surface (Fig. 1-1 (c)).

1-3-1. Organic-Thin Insulator Interfaces

It has been reported that the electronic structures of OMs on thin insulators are strongly affected by that of the underlying conductive substrate [13-18]. The energy level alignment is also determined on the basis of IDIS model (Fig. 1-3), as proposed by Heilander et al. [18]. A VL shift is given by the energy difference between the CNL of a molecule and the effective work function (Φ_{eff}) of insulator-metal. The effective work function is estimated by

$$\Phi_{\mathrm{eff}} - \mathrm{CNL}_{\mathrm{insulator}} = S(\Phi_{\mathrm{metal}} - \mathrm{CNL}_{\mathrm{insulator}}). \tag{1-4}$$

In the combination of Eq. (1-2) and (1-3), the VL shift at an OM-thin insulator interface depends on the effective work function of an insulator-metal system.

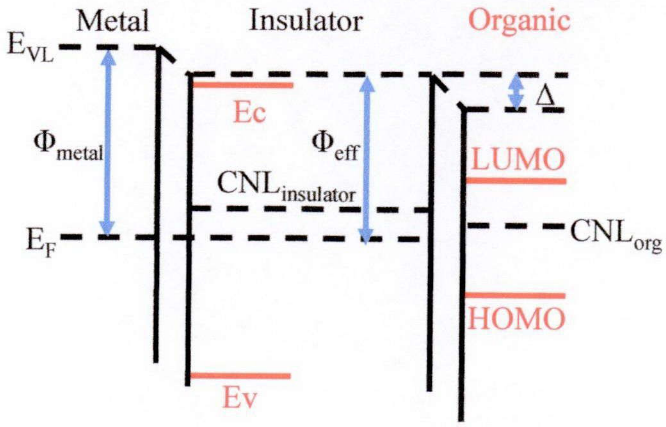

Figure 1-3. Energy diagram at an organic film on thin insulating film grown on metal substrate.

1-3-2. Organic-Thick Insulator Interfaces

Since a conventional photoemission spectroscopy technique causes charging in OMs grown on thick insulators, electrostatic force microscopy (EFM) and KPFM have been carried out to analyze the energy level [16,19-21]. Chen et al. have shown that the interface between a PEN monolayer and SiO_2 (50 nm in thickness)/n-Si exhibits a VL shift on the basis of EFM results [16]. They proposed that the origin of this VL shift was the charge transfer between PEN and SiO_2, and/or the polarization in PEN. Puntambeckar et al. carried out KPFM studies of PEN and N, N'-dioctyl-3,4,9,10-perylenedicarboximide (PTCDI-C8) on SiO_2 (300 nm in thickness)/p-Si [19]. They observed the downward and upward VL shifts of PEN and PTCDI-C8, respectively. Since PEN is typically regarded as an electron donor and PTCDI-C8 as an acceptor, the results were attributed to the difference in the direction of electron transfer. Although charge transfer has been suggested to occur between molecules and thick insulators, this project still remains controversial since charge transfer is unlikely to occur between molecules and the underlying conductive materials through thick insulators.

In Chapter 4, I will show the KPFM of organic films on 300-nm-thick thermal oxide. The KPFM results have revealed that the VL shift at an OM-thick insulator interface originates from the dipole in OMs induced by surface charges. I also denote the effect of alkyl chain with an induced dipole, the length dependence of a VL shift, and the multilayer effect on a VL shift.

1-4 Organic/Organic Interfaces

The energy level offsets at O-O interfaces are crucial parameters for the performance of organic devices. In particular, it is essential to understand the properties of a donor-acceptor (D-A) interface since the successive layer of these molecules is utilized in organic devices. Intensive research has revealed that the VL shift also occurs at D-A interfaces, which is associated with the formation of an interfacial dipole layer [2-3, 22-25]. It has been suggested that electron transfers from donor to acceptor determine a VL shift (Fig. 1-3). The charge transfer between donor and acceptor molecules has also been explained by the IDIS model [26,27]. However, this model ignores the exact contact geometry at the interface and the molecular packing, which exhibits the extreme sensitivity of electronic interactions.

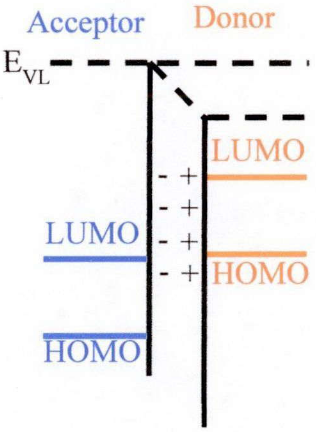

Figure 1-4. Energy diagram of a D-A interface. Donor and acceptor molecules are positively and negatively charged, respectively, at the interface due to charge transfer.

It is important to investigate the orientation dependence of electronic structure at a D-A interface. Some theoretical calculations predict that the charge transfer occurs, only when the π orbital of one molecule is faced with that of the other (Fig. 1-4(a)) [28-30]. This demonstrates that the effect of polarization has an important role in determining the origin of VL shift in the hetero-layer when each π orbital is separated (Fig. 1-4(b)).

Experimental effort has also been exerted to clarify the structural dependence of electronic structures at the D-A interface. Chen et al. fabricated the hetero-layers of copper phthalocyanine (CuPc) and perfluoro-CuPc with face-to-face and head-to-tail conformations, and measured the electronic structures by using UPS [31]. The measurements indicate that charge transfer occurs at the interfaces with both orientations. The charge transfer of the head-to-tail orientation was larger than that of face-to-face because of the energy levels modified by the effect of the local dipole. On the other hand, Duhm et al. studied the electronic properties of pentacene (PEN)/perfluoropentacene (PFP) and PFP/PEN on SiO_2 with head-to-tail orientation [32]. Each energy level had no shift in the growth of the hetero-layer. This suggests that charge transfer can be ignored, since the hybridization between σ orbitals was small.

The experimental discrepancies are considered to be attributable to the incomplete preparation of the D-A interfaces. There co-exist head-to-tail and face-to-face conformations in the films. In Chapter 5, I have fabricated the hetero-monolayer of PEN and PFP with head-to-tail and face-to-face conformations, and studied each origin of VL shifts at D-A interfaces by using KPFM.

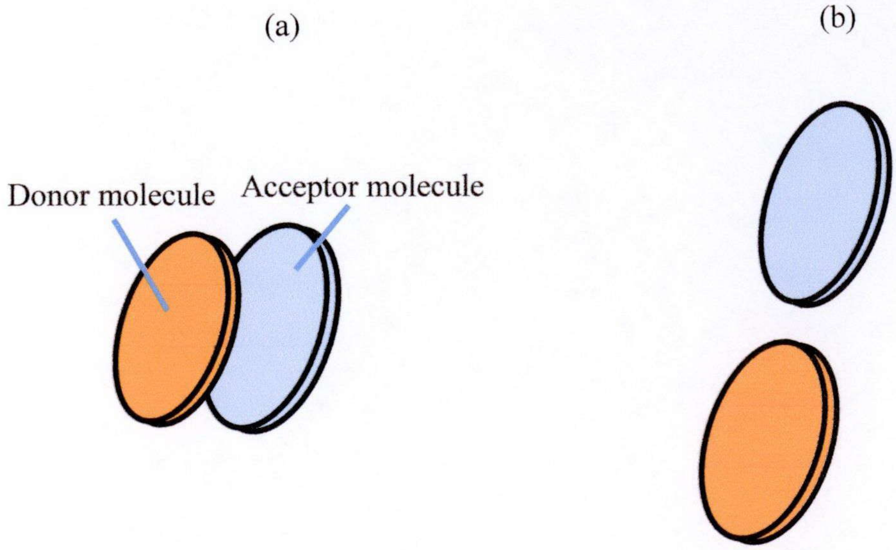

Figure 1-5. Illustration of hetero-junction with (a) face-to-face and (b) head-to-tail conformations.

1-5 Outline of Doctoral Thesis

The basic concept of KPFM employed for the project will be introduced in Chapter 2. The experimental methods will be denoted in Chapter 3. Following that, the KPFM of organic monolayers on silicon oxides will be shown, and the origin of the VL shift at an O-I interface will be discussed in Chapter 4. The geometric effects with the energy alignment at D-A interfaces will be presented in Chapter 5. Finally, a summary of these experiments and an overlook will be given in Chapter 6.

Chapter 2

Basic Principle of Kelvin Probe Force Microscopy

2-1 Historical Introduction of Scanning Probe Microscopy

The development of Scanning Probe Microscopy (SPM) was initiated in 1982 when Binnig and Rohrer invented the Scanning Tunneling Microscope (STM) [33]. This apparatus made it possible for the first time to observe single atoms on metallic surfaces in real space. Many spectacular high-resolution images of metallic and semi-conducting surfaces were published during the following years [34-37]. Binnig and Rohrer were rewarded for their pioneering invention with the Nobel Prize in 1986. Despite all euphoria, there exist some restrictions of the STM technique. Since the STM measurement depends on a small tunneling current flown between a metallic tip and a sample, the application was limited to electrically conductive materials.

It was also found that atomic forces act in tunneling distance [38,39], which motivated Binnig to develop a microscope that uses those forces as a detection signal. Together with Quate and Gerber, a prototype of the Atomic Force Microscope (AFM) was built in 1986 [40]. In contrast to the STM, the AFM is available for not only conductive but also insulating materials.

The heart of the AFM is composed of a tip attached to a cantilever (Fig. 2-1(a)). The cantilever becomes slightly bent by the forces at a small tip-sample separation. The force is given by a model of the Lennard-Jones potential (Fig. 2-1(b)). The Lennard-Jones potential is described by

$$U(r) = 4\varepsilon\left[\left(\frac{\sigma}{r}\right)^{12} - \left(\frac{\sigma}{r}\right)^{6}\right], \tag{2-1}$$

where $U(r)$ is potential energy, r is distance, ε is the depth of the potential well, and σ is the distance at which the potential is zero. Pauli repulsion acts at a short range owing to overlapping electron orbital while attractive force acts at a long range. AFM is classified into static mode (contact mode) and dynamic mode (Tapping Mode and Non-Contact Mode) according to the distance between the tip and sample (Fig. 2-1(b)).

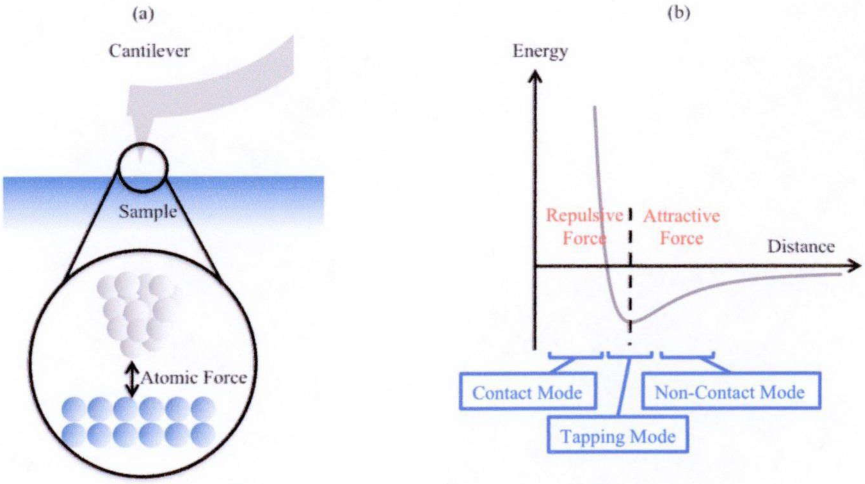

Fig. 2-1. (a) Schematic view of basic AFM system. (b) Lenard-Jones Potential. The repulsive force acts in the region below the dashed line, while the attractive force acts in the region by the upper dashed line.

2-1-1. A Static Mode in AFM Measurements

In the static mode, the tip is brought into mechanical contact with the sample. The tip displacement is used as a feedback signal to keep the forces constant during the scan. The change of the tip position results in a topographical map of the surface. However, because of the close proximity to the sample, soft materials are scratched by a tip.

2-1-2. A Dynamic Mode in AFM Measurements

In the dynamic mode, the cantilever is excited perpendicular to the surface. Typically, the spring constant of the cantilever is from several 10 N/m to several 100 N/m. High values are desired in order to avoid the 'jump into contact' effect [39]. The dynamics of a vibrating cantilever yields to feedback including information about the force between the tip and surface. In dynamic AFMs, the amplitude and frequency shift are used as a feedback parameter to track the topography of the surface.

Martin et al. have pioneered the amplitude modulation (AM) mode, that is, the tapping mode [41]. AM-AFM is widely used in air and liquid environments. The cantilever is excited at a frequency value with oscillation amplitude ranging between 10 and 100 nm. Usually, the frequency value is chosen to be slightly higher than the resonant frequency of the cantilever. The signal in the AM-mode corresponds to the change of the oscillation amplitude. The tip-cantilever ensemble is approached towards the sample until the oscillation reaches a set point value. An image is formed by scanning the tip on the sample, as the amplitude is kept at a set point value.

In the FM-mode, the non-contact mode, developed by Albrecht et al. [42], the cantilever is driven at its resonance frequency with amplitude of several nm. The phase between the driving amplitude and the oscillation amplitude is kept constant at the optimum value and the excitation is controlled in a way to keep the oscillation amplitude constant. A change in the force gradient causes the shift in the oscillation frequency, which are detected by a FM demodulator. The resulting frequency shift is used as the feedback signal to control the distance. Additionally, most experiments in ultrahigh vacuum (UHV) are performed in

FM-AFM, which allows to the first true atomic resolution [43] in UHV.

2-2. Kelvin Probe Force Microscopy

2-2-1. Application of AFM

Many progresses of AFM have been made to obtain not only an atomic force but also a friction force [44,45], a magnetic force [46-48], an electrostatic force [49-51], a chemical bonding [52], and so on. Kelvin probe force microscopy (KPFM) is one of applicable AFMs for measuring work function and surface potential. A KPFM imaging with atomic resolution is reported in combination with NC-AFM [53,54].

2-2-2. The Kelvin Principle

The Kelvin probe force microscopy derives from the method developed by Lord Kelvin in 1898 [55]. The Kelvin methods are based on measurements with a probe and a sample, and determine the difference in work function between two materials, that is, a contact potential difference (CPD). The contact potential difference V_{CPD} between two materials is given by

$$V_{\mathrm{CPD}} = \frac{1}{\mathrm{e}}\left(\Phi_1 - \Phi_2\right) = \frac{\Delta\Phi}{\mathrm{e}}, \qquad (2\text{-}2)$$

where Φ_1 and Φ_2 are the work functions of the two materials.

Figure 2-1 shows the principle of the measurements. As two conductive materials are separated, the energy diagrams are located with respect to a common vacuum level (VL) energy (E_{VL}), as shown in Fig. 2-1(a). By electrically connecting the two materials, the Fermi energy aligns through charge transfer from one material to the other (Fig. 2-2(b)). The potential difference V_{CPD} forms an electric field between the two materials. By applying a voltage $V_{DC} = V_{CPD}$, the potential difference can be compensated for, and the electrostatic fields between the materials are nullified (Fig. 2-2(c)).

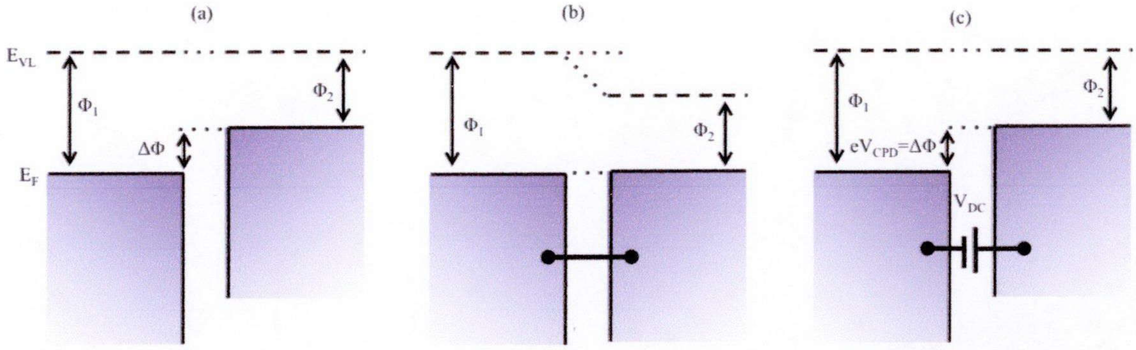

Fig. 2-2. Schematic view of two materials with different work functions. In (a) the materials are not connected and have the same vacuum energy E_{VL}. In (b) the materials are electrically connected and the Fermi energy levels E_F are equalized, resulting in the contact potential V_{CPD}. Applying a DC-voltage V_{DC} in (c) compensates for this contact potential.

The original Kelvin method is based on the modulation of a plate capacitor between a probe and a sample [55]. The two materials were brought close together, leaving a very thin gap between them. The distance between the two plates is modulated with a periodic oscillation at the frequency ω. This modulation leads to a current given by

$$I(t) = (V_{DC} - V_{CPD})\Delta C \cos \omega t\ . \tag{2-3}$$

ΔC is hereby the variation of the capacitance caused by the oscillation. To determine the contact potential difference, a bias voltage V_{DC} is applied to the system. This voltage is adjusted to a value at which the electric field in the gap becomes zero, resulting in no current. Although this method has a high accuracy in the determination of potentials, it is not possible to obtain the spatial dependence of CPD.

2-2-3. Principle of Kelvin Probe Force Microscopy

Kelvin probe force microscopy (KPFM) combines AFM with the original Kelvin method. Instead of a modulation current in the original Kelvin method, electrostatic force between the tip and a sample is measured in KPFM.

The first approach of KPFM goes back to Weaver and Abraham in 1991 [56]. The electrostatic force (F_{es}) between the tip and sample is given by

$$F_{\mathrm{es}} = \frac{1}{2}\frac{\partial C}{\partial z}\left(V_{\mathrm{bias}} - V_{\mathrm{CPD}}\right)^2, \tag{2-3}$$

where z is the distance between a tip and a sample, V_{bias} is the voltage applied between the cantilever and the sample, and V_{CPD} is the contact potential difference. To separate electrostatic and atomic forces, an additional AC-voltage V_{AC} with the frequency ω is applied between the tip and sample. The resulting potential difference

$$V_{\mathrm{bias}} = V_0 - V_{\mathrm{AC}}\sin(\omega t), \tag{2-4}$$

with $V_0 = V_{\mathrm{DC}} - V_{\mathrm{CPD}}$ can be inserted into equation (2-3), which results in three additive components of the electrostatic force [57]:

$$F_{\mathrm{es}} = -\frac{V_{\mathrm{bias}}^2}{2}\frac{\partial C}{\partial z} = F_{\mathrm{DC}} + F_{\omega} + F_{2\omega}, \tag{2-5}$$

$$F_{\mathrm{DC}} = -\frac{\partial C}{\partial z}\left[\frac{1}{2}\left(V_{\mathrm{DC}} - V_{\mathrm{CPD}}\right)^2 + \frac{V_{\mathrm{AC}}^2}{4}\right], \tag{2-6}$$

$$F_{\omega} = -\frac{\partial C}{\partial z}\left[\frac{1}{2}\left(V_{\mathrm{DC}} - V_{\mathrm{CPD}}\right)^2 V_{\mathrm{AC}}\sin(\omega t)\right], \tag{2-7}$$

$$F_{2\omega} = +\frac{\partial C}{\partial z}\frac{V_{\mathrm{AC}}^2}{4}\cos(2\omega t), \tag{2-8}$$

with $\partial C/\partial z$ being the capacitance gradient between the tip and sample. Compensating for the contact potential by setting $V_{DC} = V_{CPD}$ leads to a nullified first harmonic F_{ω} of the electrostatic force (Eq. 2-7). Then, the DC part of the force F_{DC} becomes proportional to V_{AC}^2

(Eq. 2-6), causing a minimal static force and a constant bending of the cantilever. The second harmonic equation (2-8) contains the capacitance gradient and can therefore be used to perform capacitance spectroscopy at 2ω. The electrostatic interaction is obtained by tuning ω of V_{AC} to the second resonance of the cantilever with a lock-in technique and a feedback circuit, while a cantilever scans the surface of a sample.

2-2-4. KPFM Measurements of Adsorbates on a Substrate

Usually, a KPFM is used to obtain a VL shift by measuring the spatial CPD of adsorbate and substrate. Figure 2-3 shows a typical example of a KPFM image for an inorganic semiconductor on metal. The alignment of Fermi levels between the semiconductor and the metal interface forms an electric dipole at the interface, causing a VL shift. In this Thesis, the interface dipole pointing from the surface to the vacuum is defined as ‘‘positive’’, which corresponds to a downward VL shift. A downward VL shift is expressed as ‘‘negative’’ sign ($\Delta < 0$). While the cantilever scans the sample, the local CPD of metal and semiconductor/metal are detected in each position. The difference in CPD between metal and semiconductor/metal corresponds to the VL shift, which is reflected as a contrast in a KPFM image.

A KPFM technique has been applied to organic materials on inorganic substrates. Zerweck et al. carried out the KPFM of C_{60} monolayers on Au, Cu, and Ag [58]. They showed that the VL shifts measured by KPFM and UPS coincide with each other. Furthermore, the application of KPFM to insulating materials was also established [59,60]. The insulating materials are put on a conductive substrate to apply a bias voltage between the conductive cantilever and substrate. It is known that the electric field applied between a conductive cantilever and substrate does not decay in an insulating material owing to the sharpness of the cantilever. Currently, KPFM has been used for insulator substrates with thicknesses of ~1 mm.

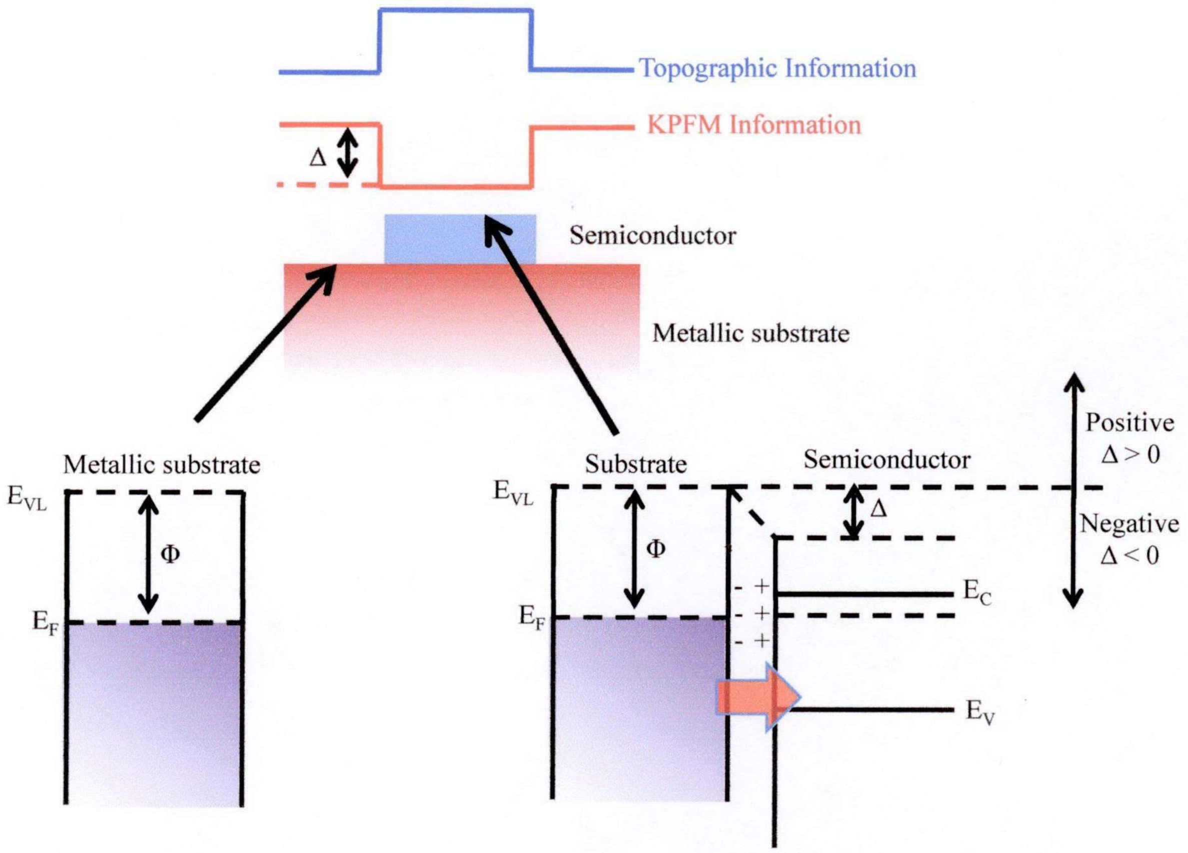

Fig. 2-3. A schematic view of KPFM observation of semiconductor on metal substrate. The VL shifts occur at a metal-semiconductor interface. In KPFM measurements, the contrast corresponds to the VL shift (Δ). A positive value of Δ shows an upward VL shift and a negative value of Δ shows a downward VL shift with respect to a substrate.

Chapter 3

Experimental Setup

3-1. Electric Circuits of AFM and KPFM Systems

3-1-1. Electric Circuits of an AFM Machine

In this Thesis, a commercial JEOL JSPM 5200 AFM was operated with a tapping mode at room temperature. The oscillation amplitude of a cantilever yields to feedback including the topographic information. The AFM consists of a cantilever with a tip, a sample stage and an optical beam deflection, as shown in Fig. 3-1. The cantilever is oscillated by using the piezo attached to the cantilever holder. The beam deflection is utilized to obtain the displacement of the cantilever. Laser light irradiated from a solid state diode is reflected off the back of the cantilever and is collected by a position detector consisting of four spaced photodiodes whose output signal is detected by a differential amplifier. The vertical photodiode (A-B) provides the signal of the cantilever parallel to a scanning direction, while the lateral one (C-D) is available to obtain the signal of the cantilever perpendicular to a scanning direction. The vertical signal provides topographic information of a sample.

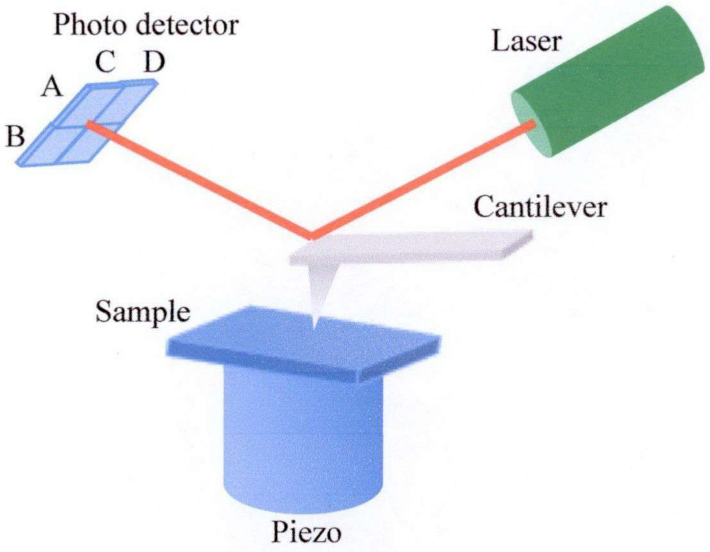

Fig. 3-1. A model of the beam-detection method. The light reflected by the cantilever is detected by a four-divided photo detector, which is able to record normal and lateral displacement of the cantilever.

3-1-2. Electric Circuits of a KPFM System

The schematic view of the electric circuit of KPFM is shown in Fig. 3-2. AC bias voltage is applied to a tip from the lock-in amplifier (Boston Electronics). The cantilever amplitude of the response to the electrostatic force induced by the AC bias voltage is measured by photo-diode. The ω component of this signal is proportional to V_{DC} - V_{CPD}, and is taken thorough lock-in amplifier. The KPFM control module is used to add a DC offset to the bias modulation, which was adjusted to null the V_{DC} - V_{CPD}. The V_{DC} is plotted in a KPFM image.

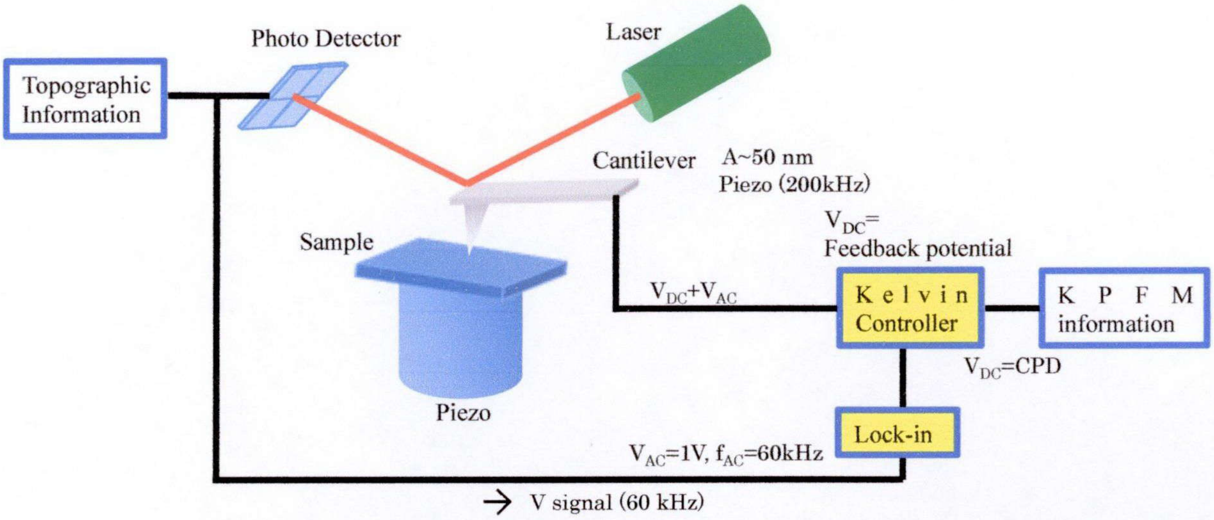

Fig. 3-2. The electrical circuit of KPFM measurements by using lock-in amplifier.

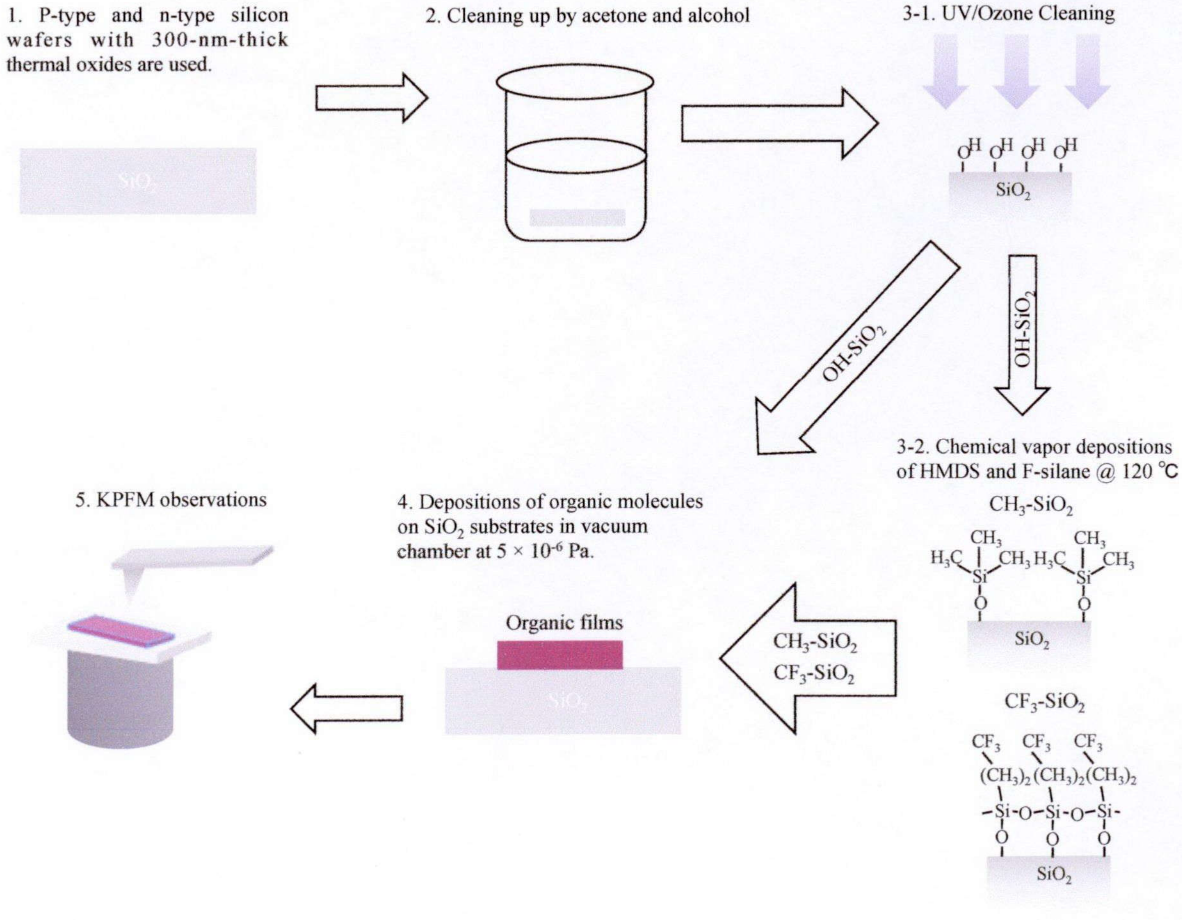

Fig. 3-3. Experimental procedures from a sample preparation to a KPFM observation.

3-2. Sample Preparation

The procedure from sample preparation to KPFM observation is summarized in Fig. 3-3.

3-2-1. Substrates

High-doped p-type and *n*-type of silicon wafers (0.01 Ωcm) covered with 300-nm-thick thermal oxides were used as substrates. The substrates were cleaned in acetone and isopropyl alcohol. The thermal SiO_2 was cleaned by an UV-ozone method [61]. Through this cleaning, organic contaminations on the substrate were removed, and the thermal SiO_2 surface was terminated with an OH group. The surface showed a water contact angle of almost 0° because of its hydrophilic property. Hexamethyldisilazane (HMDS) and trifluorosilane (CF_3-silane) were covered on the substrate by chemical vapor deposition [62]. The substrate was placed together with the HMDS and CF_3-silane liquid in the container. The container was heated in an oven at 120 ℃ for 30 minutes. The substrates were cleaned in acetone and isopropyl alcohol again. The silane termination of SiO_2 was confirmed by water contact angles of 60 ° (HMDS) and 70 ° (CF_3-silane) [63,64]. The thermal SiO_2 was then quickly loaded into a vacuum chamber. The HMDS and CF_3-silane terminated substrates are named CH_3- and CF_3-SiO_2 with the chemical species on the surface respectively.

3-2-2. Vacuum Depositions of Organic Molecules on SiO_2 Substrates

The schematic view of the vacuum chamber is shown in Fig. 3-4. The chamber was pumped at the pressure of 5×10^{-6} Pa with a combination of rotary and turbo molecular pumps. Four molecular sources were located in the chamber. The target molecules were deposited with the substrate heated by a ceramic heater. The deposition rate and the coverage were controlled with a frequency shift of a quartz oscillator. The shutter was opened by hand, when the frequency shift reached the desired value.

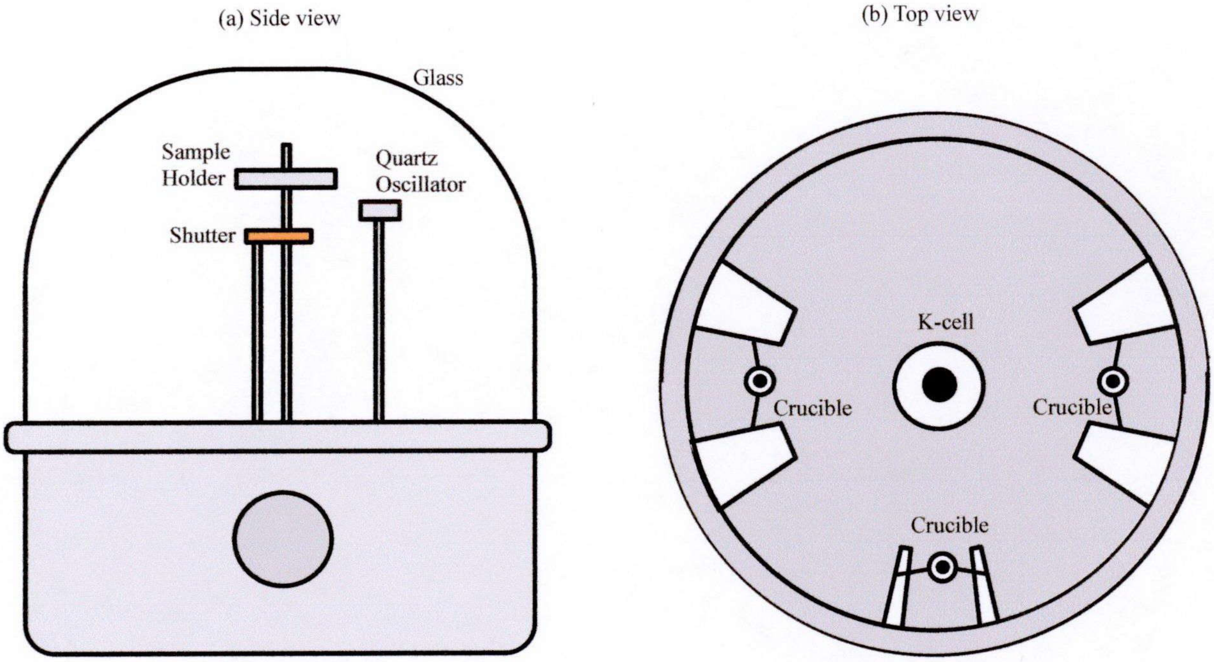

Fig. 3-4. (a) Side and (b) top views of the deposition chamber. One K-cell and three crucibles are prepared in the chamber.

3-2-3. Organic Molecules

Typical plate-like and alkylated plate-like conjugated molecules are used in this Thesis (Table 3-1). Pentacene (PEN), α-quinquethiophene (5T), α-sexithiophene (6T), α-septithiophene (7T), and α,ω-dihexyl-sexithiophene are donor (D) molecules, while perfluoropentacene (PFP) and ditridecyl-3,4,9,10-perylenetetracarboxylic diimide (PTCDI-C13) are acceptor (A) molecules. It has been reported that the former and latter molecules show *p*- and *n*-types of OFET characteristics with high mobility, respectively. PEN, 6T, DH-6T, and PTCDI-C13 were purchased from Aldrich, 5T and 7T from Wako Chemical, and PFP from Kanto Denka Kogyo.

These molecules were purified by vacuum sublimation prior to use. Table 3-2 shows substrate materials, molecular species, coverage, and substrate temperature in the species prepared in each section. In Chapter 5, two kinds of different molecules were separately deposited on OH-SiO_2 to prepare a D-A interface. The second molecules were deposited at room temperature (RT) to avoid mixing with the first ones.

Table. 3-1. Organic molecules used in our experiments.

Molecular Name	PEN Pentacene	PFP Perfluoropentacne	DH-6T α,ω-dihexyl-sexithiophene	PTCDI-C13 ditridecyl-3,4,9,10-perylenetetracarboxylic diimide
Chemical Formula	$C_{22}H_{14}$	$C_{22}F_{14}$	$C_{36}H_{38}S_6$	$C_{50}H_{66}N_2O_6$
Molecular Weight	278	530	663	790
Molecular Shape		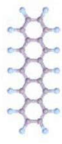		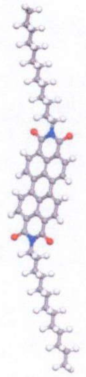
HOMO	5.0 eV [32, 65]	6.7 eV [65]	4.7 eV [6]	6.3 eV [69]
LUMO	2.9 eV	5.0 eV	2.9 eV	4.2 eV
Sublimation Temperature	150 ℃	150 ℃	400 ℃	420 ℃
Mobility	5.5 cm²/Vs [66-68]	0.2 cm²/Vs [65]	1.0 cm²/Vs [70]	2.1 cm²/Vs [71]
Color	Purple	Purple	Orange	Red

Molecular Name	5T α-quinquethiophene	6T α-sexithiophene	7T α-septihiophene
Chemical Formula	$C_{20}H_{12}S_5$	$C_{24}H_{14}S_6$	$C_{28}H_{16}S_7$
Molecular Weight	412	495	578
Molecular Shape		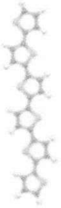	
HOMO	5.1 eV*	5.0 eV*	4.7 eV*
LUMO	2.8 eV	3.2 eV	3.0 eV
Sublimation Temperature	150 ℃	280 ℃	370 ℃
Mobility	0.05 cm^2/Vs [72]	0.08 cm^2/Vs [72]	0.13 cm^2/Vs [72]
Color	Yellow	Orange	Orange

Table. 3-2. Substrate materials, molecular species, coverage, and substrate temperature used in each sample.

	Substrates	First Molecule	Coverage (ML)	Substrate Temperature (℃)	Second Molecule	Coverage (ML)	Substrate Temperature (℃)
Sec. 4-2	(Thermal) OH-SiO_2/*p*-Si (Thermal) OH-SiO_2/*n*-Si	PEN	0.7	60			
Sec. 4-4	(Thermal) OH-SiO_2/*n*-Si	PEN	0.7				
Sec. 4-6	(Thermal) CH_3-SiO_2/*n*-Si (Thermal) CF_3-SiO_2/*n*-Si	PEN PFP	0.7 0.7	60 60			
Sec. 4-8	(Thermal) OH-SiO_2/*n*-Si	5T 6T 7T	0.4 0.6 0.3	80 100 120			
Sec. 4-12	(Thermal) OH-SiO_2/*n*-Si	DH6T PTCDI-C13	0.5 0.3	100 100			
Sec. 4-5-2	(Thermal) OH-SiO_2/*n*-Si (Thermal) CF_3-SiO_2/*n*-Si	PEN PFP	1.4 1.4	60 60			
Sec. 5-2-1	(Thermal) OH-SiO_2/*n*-Si	PFP	0.6	60	PEN	0.4	RT
Sec. 5-2-2	(Thermal) OH-SiO_2/*n*-Si	PEN	0.6	60	PFP	0.2	RT
Sec. 5-4	(Thermal) OH-SiO_2/*n*-Si	PFP	1.2	60	PEN	1.6	RT
Sec. 5-5-2	(Thermal) OH-SiO_2/*n*-Si	5T 6T 7T	0.5 0.6 0.4	80 100 120	PFP	0.3	RT
Sec. 5-5-4	(Thermal) OH-SiO_2/*n*-Si	6T	0.7	100	PFP	0.3	RT

---

* HOMO and LUMO levels of 5T, 6T, and 7T are calculated by DMol3.

3-2-4. KPFM Measurement

A silicon cantilever was coated with Au (20 nm)/Cr (10 nm) (MikroMasch, NSC35/Cr–Au/15). Its spring constant was 1.9 N/m. The tip diameter was 10 μm and the tip height is 40 μm. The resonance frequency was approximately 200 kHz.

KPFM was carried out in a nitrogen gas atmosphere. In an ambient condition, an unstable signal occasionally provided the reversal of the contrast in a KPFM image of Au/*n*-Si (Fig. 3-5(b)) taken simultaneously with a topographic image (Fig. 3-5(a)), because of the instability of electric field between a sample and a tip. Thus, nitrogen gas was flown into the measurement chamber at a rate below 10 ml/min, making the electric field more stable (Fig. 3-5(c)).

The KPFM signal depends on a scan speed, an AC bias voltage and the frequency. The KPFM of Au/n^{++}-Si compensates for the signal in nitrogen gas condition. The optimized scan speed, AC bias voltage, and frequency were 0.1 Hz, 1.0 V, and 60 kHz, respectively.

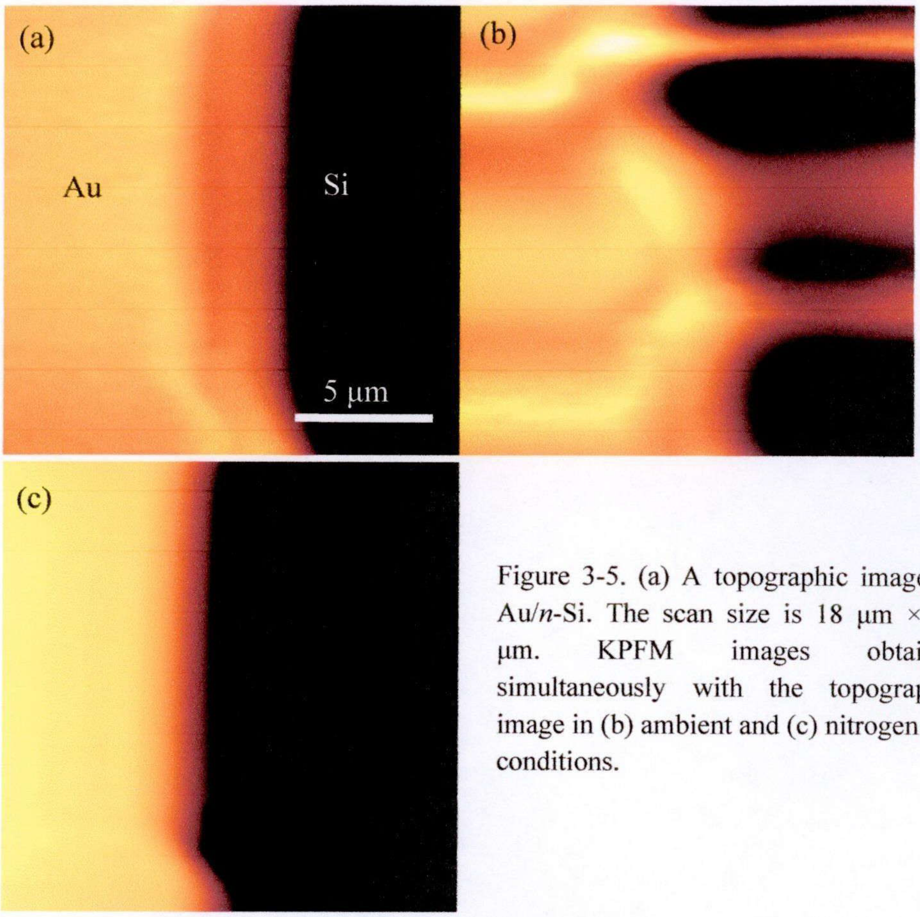

Figure 3-5. (a) A topographic image of Au/*n*-Si. The scan size is 18 μm × 18 μm. KPFM images obtained simultaneously with the topographic image in (b) ambient and (c) nitrogen gas conditions.

3-3. Calculations

DFT calculations were performed with the program DMol3 to obtain a molecular orbital [73]. A plane wave basis set was used for the valence electronic states and Vanderbilt ultrasoft pseudo-potentials were applied for the calculation of core-electron interactions. The local density approximation (LDA) was utilized.

Chapter 4

Electrostatic Properties of Organic-Insulator interfaces

4-1. Organic-Thick insulator interfaces

It has been reported that charge transfer occurs between an organic material (OM) and an underlying conducting substrate through thin insulating film [13-18]. The increase in thickness of insulating film is considered to reduce charge transfer efficiency between OM and the underlying conducting substrate. It is interesting to clarify the origin of a VL shift of organic films on the insulating oxides with a thickness enough to prevent electrons tunneling between OM and the underlying Si. In this Section, I show the KPFM of PEN on 300-nm-thick thermal SiO_2 grown on p- and n-type silicon, and studied the origin of the VL shift.

4-2. Results and Discussion of Organic-Thick Insulator Interfaces

Figures 4-1(a) and 4-1(b) show the topographic images of PEN on 300-nm-thick SiO_2/p-Si and SiO_2/n-Si, respectively. The height of the PEN films with respect to the substrate was 1.8 nm ± 0.2 nm. The height of the PEN ML is also in the range from 1.6 nm to 2.2 nm measured by AFM [74-78]. It is unclear why the values reported are larger than the molecular length (1.40 nm) and even the length estimated by taking the van der Waals radii (c.a. 1.64 nm) into consideration. In addition, the height of PEN on thermal oxides is larger than that on native oxides [74].

Figures 4-1(c) and 4-1(d) show the KPFM images of PEN MLs on thermal SiO_2/p- and SiO_2/n-Si taken simultaneously with the topographic ones, respectively. PEN MLs appeared darker than the substrates, indicating a downward VL shift. The VL shifts of PEN on both substrates were 150 mV.

Next, I discuss the origin of a VL shift at an OM-thick insulator interface. At an organic-thin insulator interface, the energy position of the OM and the insulator-underlying conductor system determines a VL shift on the basis of the IDIS model [18]. In this model, a VL shift is proportional to the effective work function of substrates. The effective work function of the background silicon of SiO_2/p-Si and SiO_2/n-Si is known to be 5.2 eV and 4.2 eV [79]. Actually, PEN on native SiO_2/p-Si and SiO_2/n-Si showed different VL shifts of -510 mV and -310 mV, respectively, in my previous experiment. On the other hand, the VL shift occurs for PEN on thermal SiO_2/p-Si and SiO_2/n-Si was the same, in spite of their effective work function. Therefore, the origin of a VL shift at an OM-thick insulator interface is not charge transfer between PEN and underlying silicon owing to the thick insulating film. This means that the IDIS model is not applicable to the system of OMs on thick insulators.

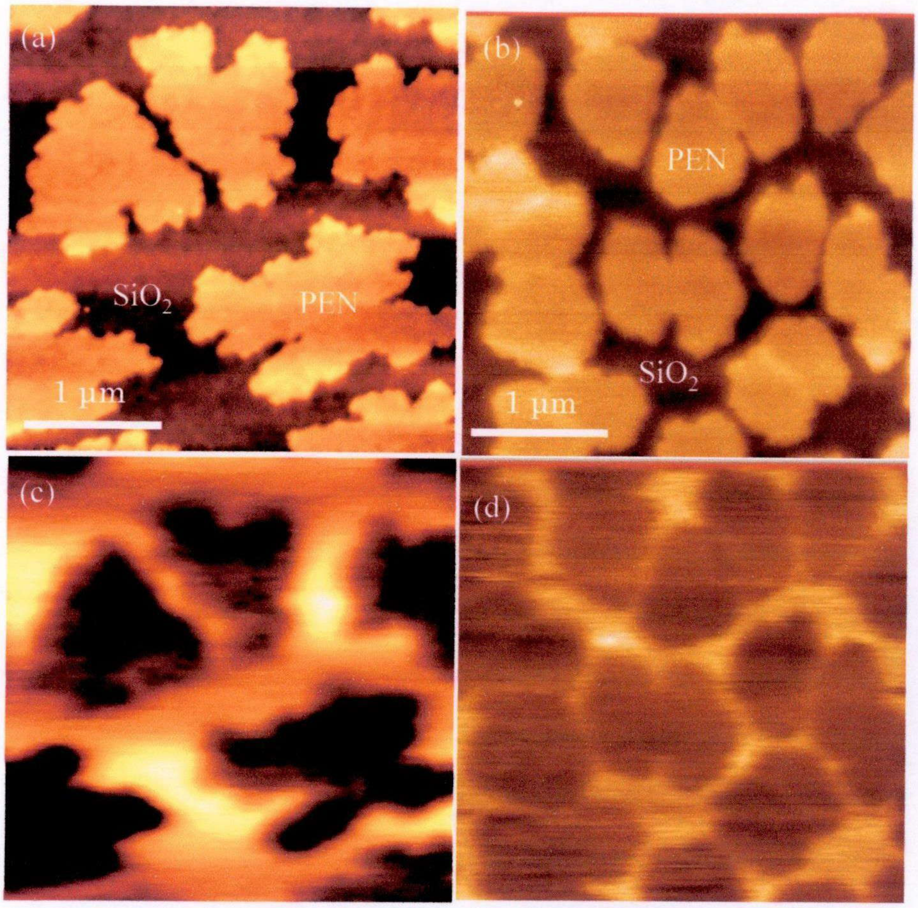

Figure 4-1. Topographic images of PEN MLs deposited on thermal oxides on (a) p- and (b) n-Si. KPFM images of PEN MLs on SiO_2/ (a) *p*- and (b) *n*-Si obtained simultaneously with topographic images. The scan size is 3 μm × 3 μm.

The electronic interaction between molecular orbitals of PEN and electronic states of SiO_2 can also be ignored, since the energy gap between these levels is significantly large: The valence band (E_v) and conduction band (E_c) are 9.0 eV and 0.1 eV, respectively [79]. The highest occupied molecular orbital (HOMO) and lowest unoccupied molecular orbital (LUMO) of PEN with respect to a VL are 5.0 eV and 2.9 eV, respectively [32,65]. Thus, I examine a direct transfer of electrons between the energy level of PEN and the charge neutrality level (CNL) of SiO_2, which is a surface states. The CNL of SiO_2 is known to be 4.9 eV [79]. Since the HOMO level of PEN is located near the CNLs of the SiO_2, it seems possible that charge transfer occurs from PEN to SiO_2. This scheme results in a downward

VL shift, which agrees with our experimental result. The energy diagram can be described in Fig. 4-2.

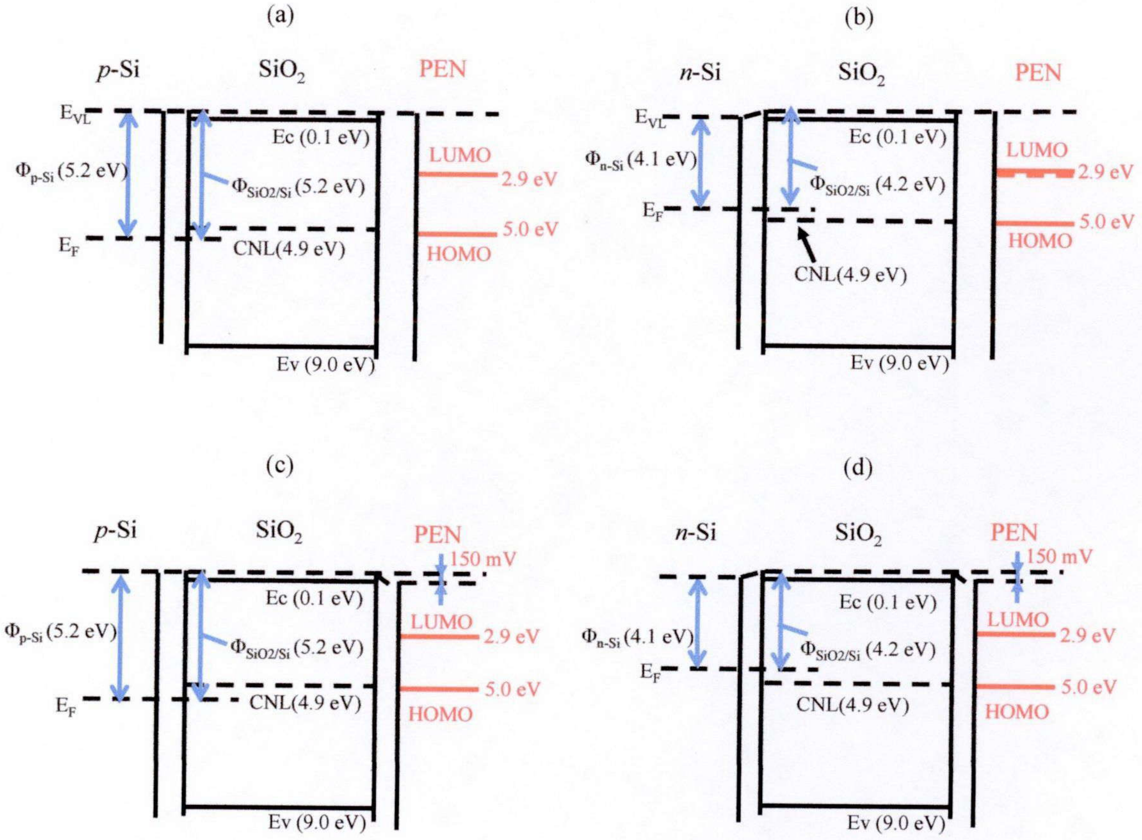

Figure 4-2. Energy diagrams at the interface PEN and thermal oxides/p-Si (a) and n-Si (b) in the separation with each other. If the charge transfer between PEN and SiO$_2$ occurs, the energy diagrams at the interface PEN and thermal oxides/p-Si and n-Si can be described in 4-2(c) and 4-2(d), respectively.

4-3. Perfluoropentacene Monolayers on Thick Insulators

The KPFM of PEN on thermal SiO$_2$/p-Si and SiO$_2$/n-Si suggests not the charge transfer between an OM and an underlying conductiing substrate, but the charge transfer occurs between an OM and an insulator. In order to verify this model, it is essential to examine the interface properties of an acceptor molecule and an insulator. Puntambeckar et al. obtained the VL shifts of PEN and N, N'-dioctyl-3,4,9,10-perylenedicarboximide (PTCDI-C8) on SiO_2 in the opposite direction. They proposed that the results were attributed to the difference in the direction of electron transfer, since PEN is typically regarded as an electron donor and PTCDI-C8 as an acceptor [18]. In this Section, I perform the KPFM of perfluoro-PEN (PFP) on 300-nm-thick thermal SiO_2/n-Si, and determine whether the charge transfer model is applicable for a VL shift at an OM-thick insulator interface or not. PFP is known to be a typical acceptor molecule with the same molecular frame as PEN.

4-4. Results and Discussion of Perfluoropentacene Monolayers on Thick Insulators

Figure 4-3(a) shows the topographic image of PFP ML on SiO_2. The height of the PFP films was 1.6 nm ± 0.2 nm, which agrees well with that reported previously [21,80]. XRD analyses revealed that the *d*(001) spacings of the film and bulk phases are 1.58 nm and 1.55 nm, respectively [81]. It is considered that the PFP molecules in ML on SiO_2 have the same orientation as those in the bulk phase. The molecular axis is inclined by approximately 18 degrees with respect to the surface normal.

Figure 4-3(b) shows the KPFM images of PFP ML taken with the topographic image (Fig. 4-3(a)). PFP ML on OH-SiO_2 appeared darker and brighter than the substrate, indicating a downward VL shift. A downward VL shift of 80 mV was observed for the ML on OH-SiO_2.

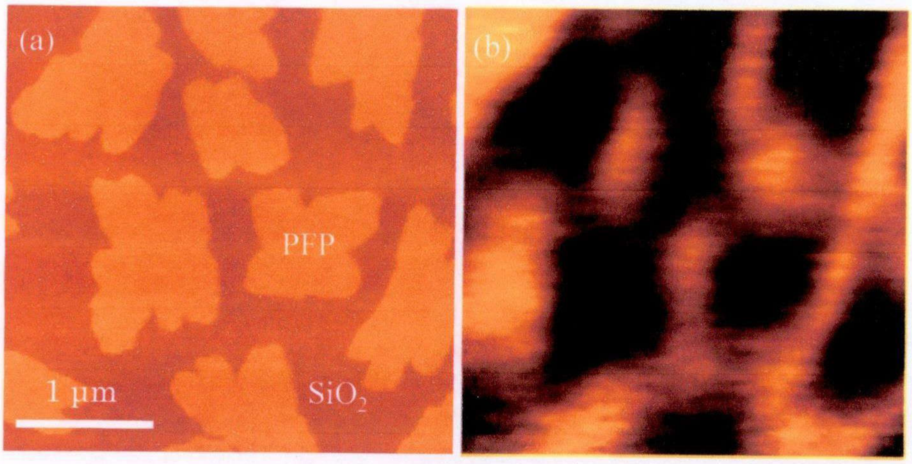

Figure 4-3. (a) Topographic and (b) KPFM images of PFP MLs deposited on SiO_2. The scan size is 3 μm × 3 μm.

Charge transfer between OMs and SiO_2 is one of the origins of VL shift at an OM-thick insulator. HOMO and LUMO of PFP are located at 6.7 eV and 5.0 eV below VL [65]. The HOMO and LUMO levels of molecules are also shown with respect to the VL of the substrates (Fig. 4-4). The CNL of SiO_2 is located near the LUMO level of PFP. Electron transfer is considered to occur from CNL of SiO_2 to the LUMO of PFP, causing an upward VL shift. Contrary to this expectation, the direction of the VL shift of PEN was the same as that of PFP in our experiments. Therefore, charge transfer between OMs and SiO_2 is not considered to be the origin of the VL shift. This indicates that an upward VL shift of PTCDI-C8 obtained by Puntambeckar's group [18] may not also originate from charge transfer. The effect of an alkyl chain on a VL shift will be denoted in Sec. 4-7 and Sec. 4-8.

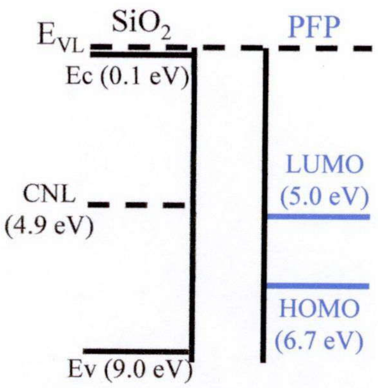

Figure 4-4. The energy diagram of PFP and SiO_2 in the separation with each other.

4-5. Organic Monolayers on Thick Insulator Terminated by Various Silanes

Chen et al. proposed not only charge transfer but also polarization for the origin of VL shift at an OM-thick insulator interface [17]. Polarization is considered to occur with charge distribution on the surface of a substrate. The termination of silane molecules on SiO_2 modifies the surface charges with the chemical species. It is important to study the effect of the charge distribution of silane molecules on a VL shift. In this Section, I show the KPFM PEN and PFP MLs on CH_3- and CF_3-SiO_2.

4-6. Results and Discussion of Organic Monolayers on Thick Insulator Terminated by Various Silanes

Figures 4-5(a) and 4-5(b) show the topographic images of the PEN MLs on CH_3- and CF_3-SiO_2/*n*-Si, respectively. The height of the PEN on both substrates films was 1.8 nm, indicating that the morphology of PEN and PFP on CH_3- and CF_3-SiO_2 is the same as that on OH-SiO_2. Since the height of the PFP films on CH_3- and CF_3-SiO_2 was approximately 1.6 nm (Figs. 4-5(c) and 4-5(d)), there is considered to be no effect of the surface modification on the film morphology.

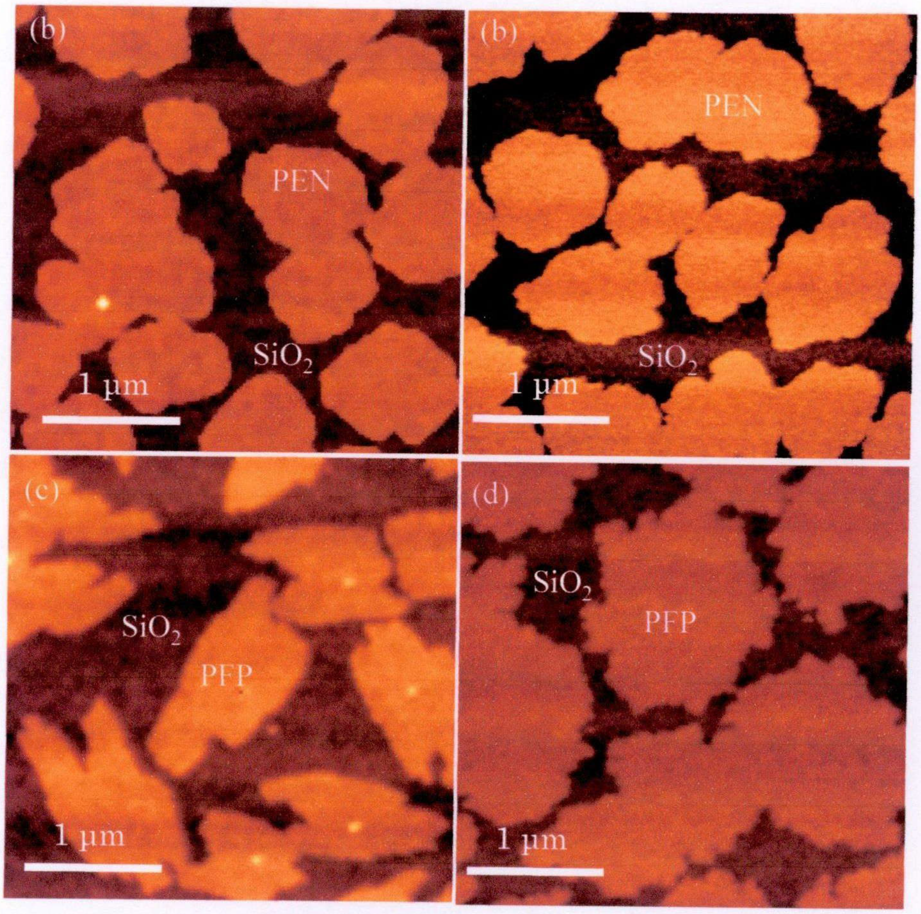

Figure 4-5. Topographic images of PEN MLs deposited on (a) CH_3- and (b) CF_3-SiO_2/*n*-Si, and PFP MLs on (c) CH_3- and (d) CF_3-SiO_2/*n*-Si. The scan size is 3 μm × 3 μm.

Figures 4-6(a) and 4-6(b) show the KPFM images of the PEN MLs on CH_3- and CF_3-SiO_2 obtained simultaneously with the topographic images in Fig. 4-6(a) and 4-6(b). The PEN ML on CH_3- and CF_3-SiO_2 appeared darker and brighter than the substrate, indicating a downward and an upward VL shift, respectively. A downward VL shift of 60 mV was observed for the ML on CH_3-SiO_2, while the film on CF_3-SiO_2 exhibited an upward VL shift of 110 mV. Figures 4-6(c) and 4-6(d) show the KPFM images of PFP on CH_3- and CF_3-SiO_2, respectively. The downward shifts of 40 mV were observed for PFP on CH_3-SiO_2, while an upward VL shift of 70 mV was observed for PFP on CF_3-SiO_2.

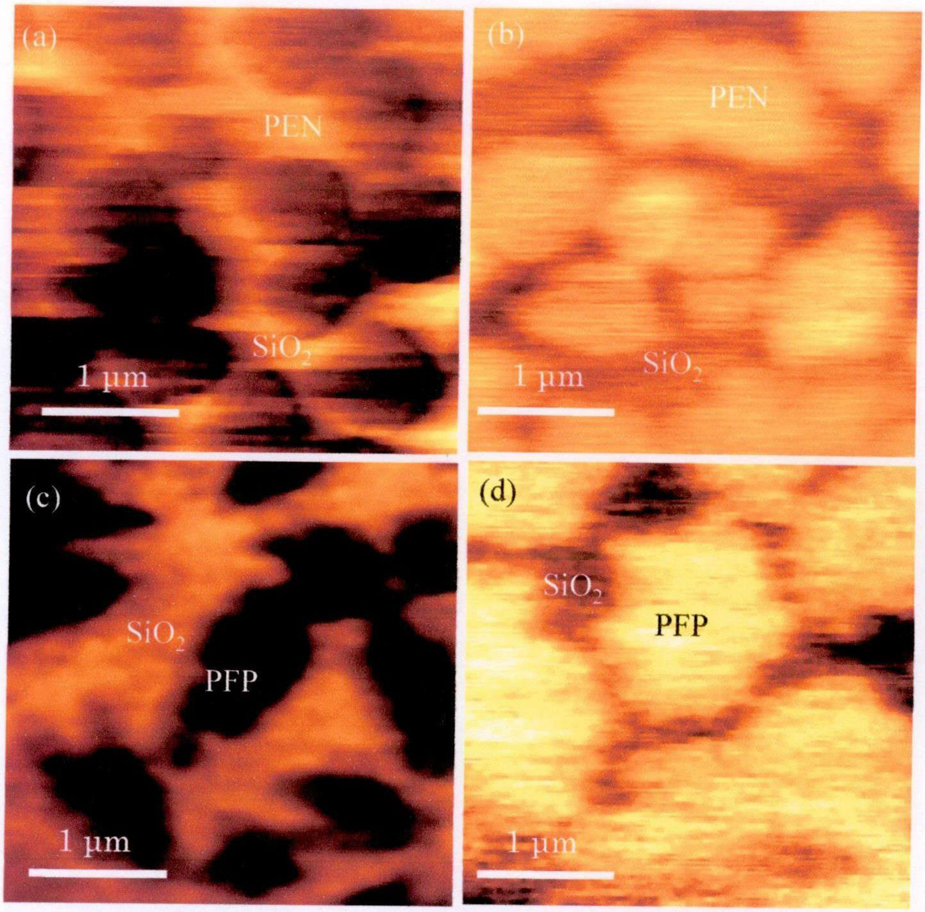

Figure 4-6. KPFM images of PEN MLs on (a) CH_3- and (b) CF_3-SiO_2/*n*-Si, and PFP MLs on (c) CH_3- and (d) CF_3-SiO_2/*n*-Si obtained with the topographic images in Fig. 4-6.

The results in Sec. 4-2, 4-4 and 4-6 are summarized in Table 4-1. First, both the PEN and PFP MLs on OH- and CH_3-SiO_2 showed a downward VL shift, while those on CF_3-SiO_2 showed an upward VL shift. Second, the shift observed for both PEN and PFP on OH-SiO_2 was larger than that on CH_3-SiO_2.

Table 4-1. KPFM results of PEN and PFP on OH-, CH_3-, and CF_3-SiO_2.

	ΔPEN (mV)	ΔPFP (mV)
OH-SiO_2	-150	-80
CH_3-SiO_2	-60	-40
CF_3-SiO_2	+110	+70

I discuss the dipoles in molecules induced by charges distributions of chemical species on SiO_2. In a hydroxyl group of OH-SiO_2, oxygen and hydrogen are charged negatively and positively, respectively, owing to the difference in electronegativity. This charge distribution induces the electric dipole in PEN. The dipole points from the surface to the vacuum, which results in a downward VL shift. The energy diagram is described in Fig. 4-7(a). Hydrogen atoms in the methyl group of HMDS are charged positively with respect to carbon atoms. This also induces the positive electric dipole in molecules that causes a downward VL shift. Since the electric dipole of a methyl group is smaller than that of a hydroxyl group, the dipole induced in molecules on CH_3-SiO_2 is smaller than that on OH-SiO_2, which agrees well with our experimental results. In the case of the monolayer on CF_3-SiO_2, F is negatively charged and C is positively charged. These charges induce negative electric dipoles in molecules. These dipoles result in an upward VL shift, which agrees well with the results obtained in the present experiment. Thus, I conclude that the dipoles induced by the charges of chemical species on SiO_2 determine the VL shift.

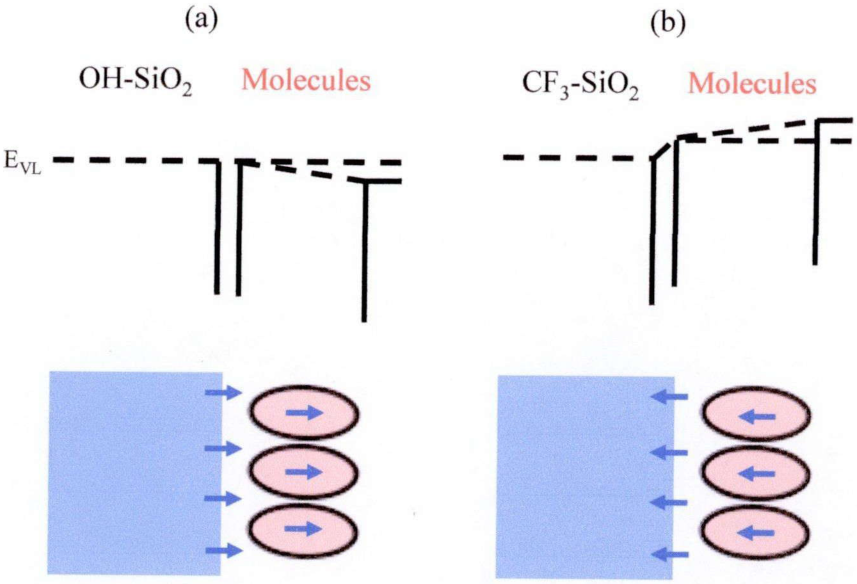

Figure 4-7. Energy diagrams at the interface of molecules on (a) OH- and (b) CF_3-SiO_2. The VL shift is attributed to a dipole in molecules induced by the surface charges. The CF_3 termination of SiO_2 shows an upward VL shift of 150 mV at the surface [62].

4-7. Oligothiophene-Thick Insulator Interfaces

The KPFM of PEN and PFP on SiO_2 showed that the dipole in molecules induced by charge of substrate surface leads to VL shift. This proposal is helpful in determining the direction of VL shift at an O-I interface. However, it is difficult to predict the magnitude of a VL shift. The VL shift is thought to depend strongly on molecular species, as observed for the difference in the shift between PEN and PFP on SiO_2.

Oligothiophene is one of the most promising molecules for applications because of their excellent electronic properties, stability under ambient conditions, and ease of chemical modification. The molecular length changes with the number of thiophene ring. n-α-thiophene (n-thiophene, nT) is described with the number (n) of thiophene units. The carrier mobility of OFET increases along with the molecular length.

In this Section, I show the KPFM of α-quinquethiophene (5T), α-sexithiophene (6T) and α-septithiophene (7T) monolayers on OH-SiO_2 and discuss their length dependence of VL shifts.

4-8. Results and Discussion of Oligothiophene - Thick Insulator Interfaces

Figures 4-8(a), 4-8(b) and 4-8(c) show the topographic images of the 5T, 6T and 7T MLs on SiO_2 with a thickness of 300 nm grown on *n*-Si, respectively. In the image, brighter areas exhibited molecular films and darker areas were the substrate. The heights of the 5T, 6T and 7T films with respect to the substrate were 2.5 nm, 2.8 nm and 3.1 nm, respectively.

It has been reported that the 5T, 6T and 7T molecules also grow in a layer-by-layer manner on SiO_2 with its molecular axis almost perpendicular to the surface. It is unclear that the values obtained are longer than the molecular length of 5T (2.2 nm), 6T (2.5 nm) and 7T (2.8 nm) with taking the van der Waals radii into account, as was discussed also for PEN on SiO_2.

Figures 4-8(d), 4-8(e) and 4-8(f) show the KPFM image of 5T, 6T and 7T monolayers on SiO_2 recorded the topographic image in Fig. 4-8(a), 4-8(b), and 4-8(c), respectively. The MLs appeared darker than the substrate, leading to downward VL shifts. The shifts for 5T, 6T and 7T showed the same, that is approximately 90 mV.

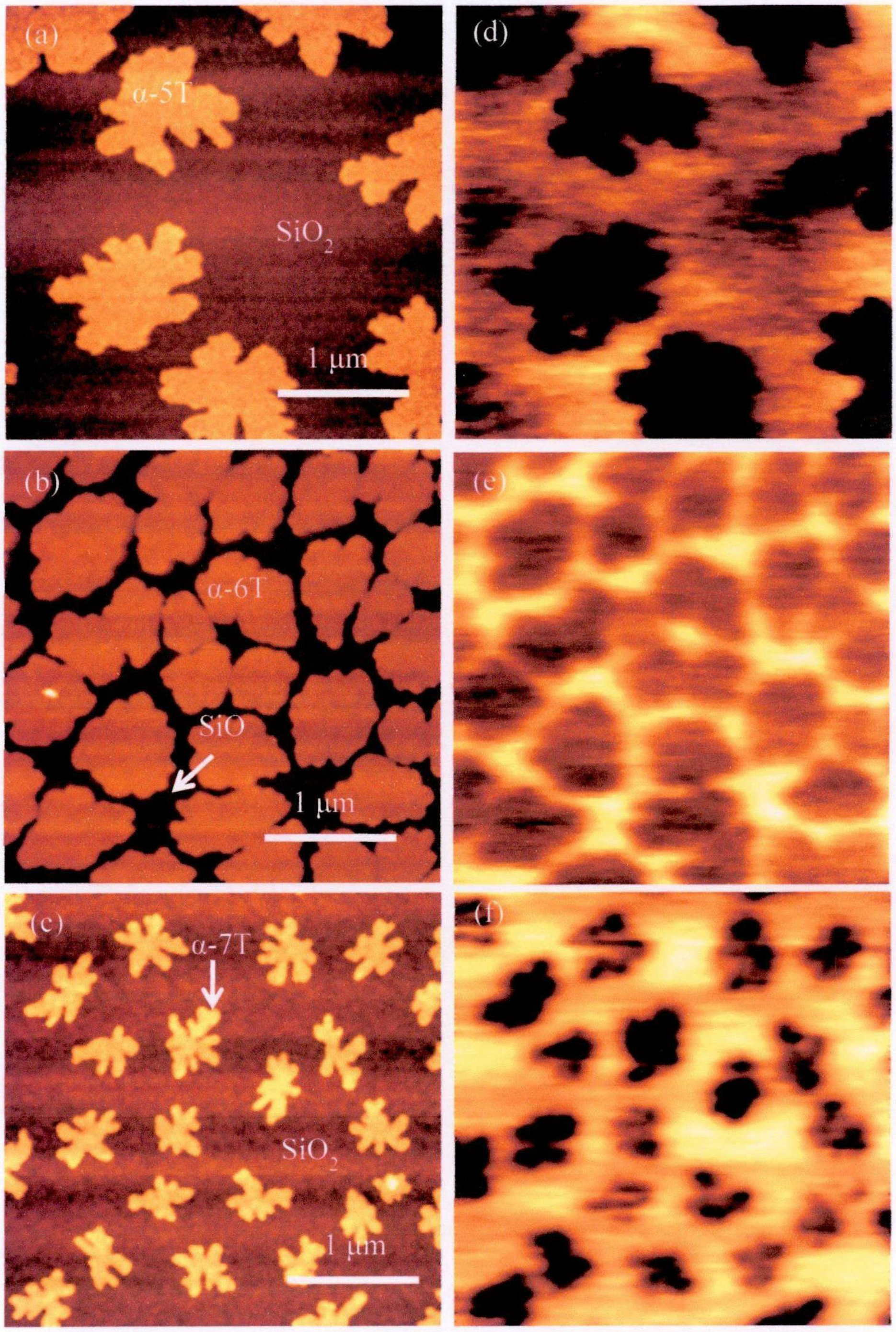

Figure 4-8. Topographic images of (a) 5T, (b) 6T, and (c) 7T deposited on OH-SiO$_2$. KPFM images (d) 5T, (e) 6T, and (f) 7T monolayers obtained simultaneously with topographic images. The scan size is 3.5 μm × 3.5 μm.

The charge transfer can be denied for the origin of VL shift in n-thiophene on SiO$_2$, since the difference between their energy level and a CNL of SiO$_2$ does not reflect the VL shift. Therefore, it is considered that the surface charge of OH-SiO$_2$ induces a positive dipole also in n-thiophene. Since the induced dipole is determined by the polarizability of molecules, it was expected that the VL shift show the length dependence. I discuss about this matter using the Helmholtz equation [4]. Helmholtz equation is described as

$$\Delta = \mu_z/\varepsilon\varepsilon_0 S = (\boldsymbol{\alpha}\bullet\mathbf{E})_z/\varepsilon\varepsilon_0 S, \tag{4-1}$$

here, ε_0 is a dielectric constant, and ε is a relative dielectric constant. S is the surface area occupied by one molecule. μ_z is a dipole moment along the direction normal to the substrate. The total dipole can be expressed as

$$\boldsymbol{\mu} = \boldsymbol{\alpha}\bullet\mathbf{E}; \tag{4-2}$$

$\boldsymbol{\alpha}$ is a polarizability tensor, and $\mathbf{E}$ is a vector of electric field.

The squares of unit-cells of 5T, 6T and 7T films are reported to be 4.64 nm^2, 4.73 nm^2 and 4.62 nm^2, respectively [72]. The electric field induced by OH-SiO_2 surface is also a constant value.

Since the VL shift showed the same for all films, the ratio between the polarizability and relative dielectric constant is given as

$$\alpha_{5T}/\varepsilon_{5T} \sim \alpha_{6T}/\varepsilon_{6T} \sim \alpha_{7T}/\varepsilon_{7T}. \tag{4.3}$$

The ratio α/ε of n-thiophene is independent of their length. In general, relative dielectric constant and polarizability tend to increase along with molecular mass, as is shown for oligoacene molecules [82,83]. It is found that the polarizability of n-thiophene increases in proportion to the relative dielectric constant, as the ring number becomes larger. Since the polarizability and relative dielectric constant are an important parameter for determining the electrostatic properties of molecule, the estimation of polarizability and dielectric constant in the combination with KPFM and Helmholtz equation is helpful in determining a VL shift.

However, there remains a problem in using Helmholtz equation. When Helmholtz equation is applied to the VL shifts of PEN on OH-, and CH_3- and CF_3-SiO_2, their relation of the relative dielectric constants is also obtained. Since PEN films have the same square of unit cell, polarizability and electric field, it is considered that the relative dielectric constant of PEN on each substrate is proportional to the VL shift obtained experimentally. This seems strange, since the relative dielectric constant is basically specific value to molecular species. Therefore, I expect that the theoretical approach is performed in order to clarify whether the Helmholtz equation is applicable for a VL shift of organic MLs on a thick insulating film or not.

4-9. Monolayers of Organic Molecules with Alkyl Chains on a Thick Insulator

The KPFM of π-conjugated molecules on SiO_2 indicates that the dipoles induced by the charges of chemical species on SiO_2 determine the VL shift. Puntambeckar et al. obtained an upward VL shift of alkylated π-conjugated molecules, PTCDI-C8, on SiO_2 and proposed that the origin of VL shift was charge transfer [18]. It is interesting to clarify the effect of the spacer between the substrate and the π system on charge transfer efficiency. In this Section, I show the KPFM of DH-6T and PTCDI-C13 to determine the origin of VL shift of molecules with alkyl chains on insulator.

4-10. Results and Discussion of Monolayers of Organic Molecules with Alkyl Chains on a Thick Insulator

Figures 4-9(a) and 4-9(b) show the topographic images of DH-6T and PTCDI-C13 monolayers deposited on OH-SiO_2. The height of DH-6T with respect to the substrate was 3.6 nm ± 0.3 nm, and that of PTCDI-C13 was 2.5 nm ± 0.3 nm, which agree with those reported previously [84,85]. The long axes of these molecules are also known to be perpendicular to the substrate surface [84,85]. It has been reported that the films consist of cofacial π-stacks.

Figures 4-9(c) and 4-9(d) show the KPFM images of the DH-6T and PTCDI-C13 monolayers on OH-SiO_2, respectively. In these images, both films appeared brighter than the substrate, indicating an upward VL shift. The shift was approximately 10 mV for both films.

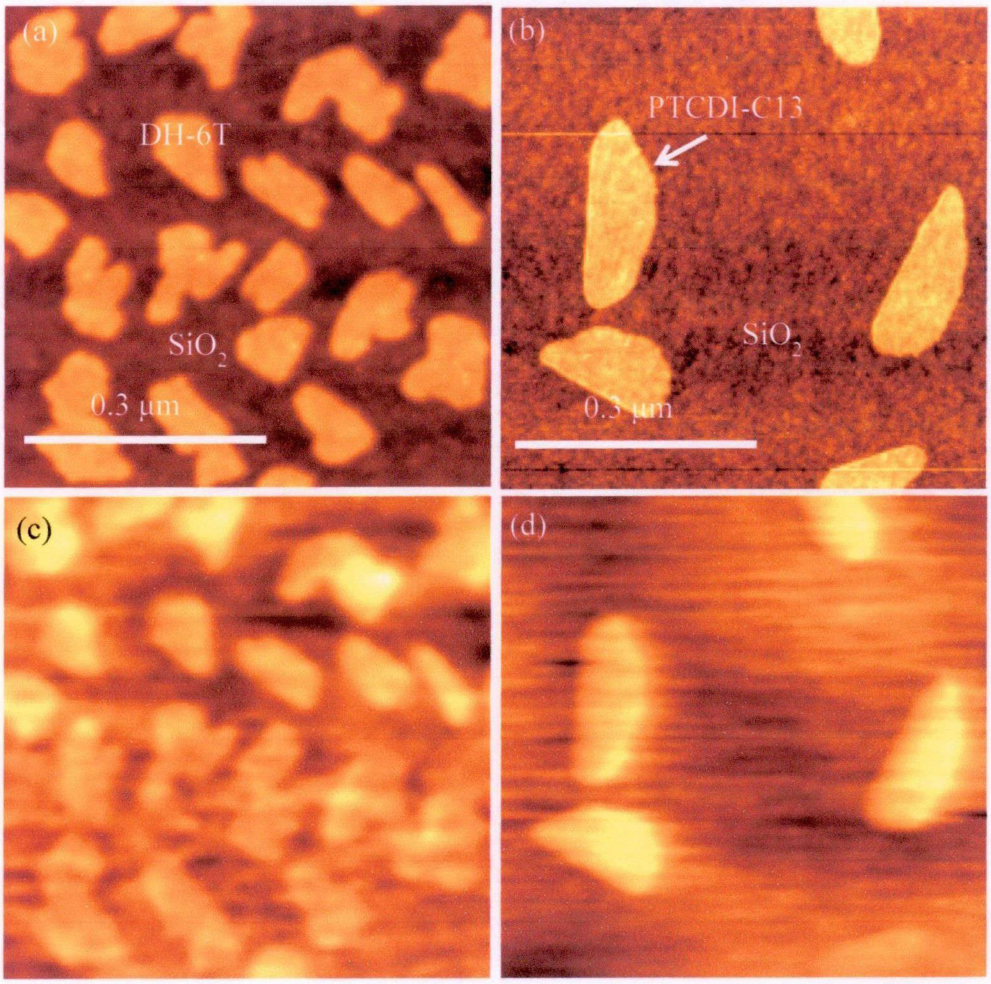

Figure 4-9. Topographic images of (a) DH-6T and (b) PTCDI-C13 monolayers deposited on OH-SiO_2. KPFM images of (c) DH-6T and (d) PTCDI-C13 monolayers obtained simultaneously with topographic images. The scan size is 0.6 μm × 0.6 μm.

Since the π-system with alkyl chains showed an upward VL shift, the origin of the VL shift could not be explained by the dipole induced. The possibility of charge transfer is also negligible, as shown below. The HOMO and LUMO levels of DH-6T are 4.7 eV and 2.9 eV

[6], and those of PTCDI-C13 are 6.3 eV and 4.2 eV [69], respectively. Compared with the CNL of 4.9 eV (OH-SiO_2), electron transfer may occur from DH-6T to SiO_2 and also from SiO_2 to PTCDI-C13, indicating VL shifts in opposite directions. Contrary to the expectation, both molecules showed an upward VL shift. Charge transfer was considered to occur less likely in the present case.

The structural deformation and/or asymmetry of the molecules on the surface also induce an intramolecular dipole. Usually the organic molecules with alkyl chains consist of a negatively charged π frame and a positively charged alkyl chain (Fig. 4-10(a)). In the case of isolated DH-6T and PTCDI-C13 molecules, the net dipole is zero, owing to the structural symmetry. The growth of these molecules on SiO_2 indicates that the upper alkyl chain leans more than the lower chain (Fig. 4-10(b)), as was pointed out by Krauss et al [86]. The structural deformation makes the direction of dipole in molecules nonparallel. The z component of dipole relates to a VL shift (z shows a direction perpendicular to the surface) on the basis of Helmholtz equation. Therefore, the dipole between a lower chain and a π frame is more dominant, resulting in an upward VL shift (Fig. 4-10(c)). It is concluded that the structural asymmetry in the molecule is a dominant factor for a VL shift at an alkylated OM-SiO_2 interface. The effect of polarization and charge transfer is weakened because of the alkyl chain inserted between substrate and the π orbital.

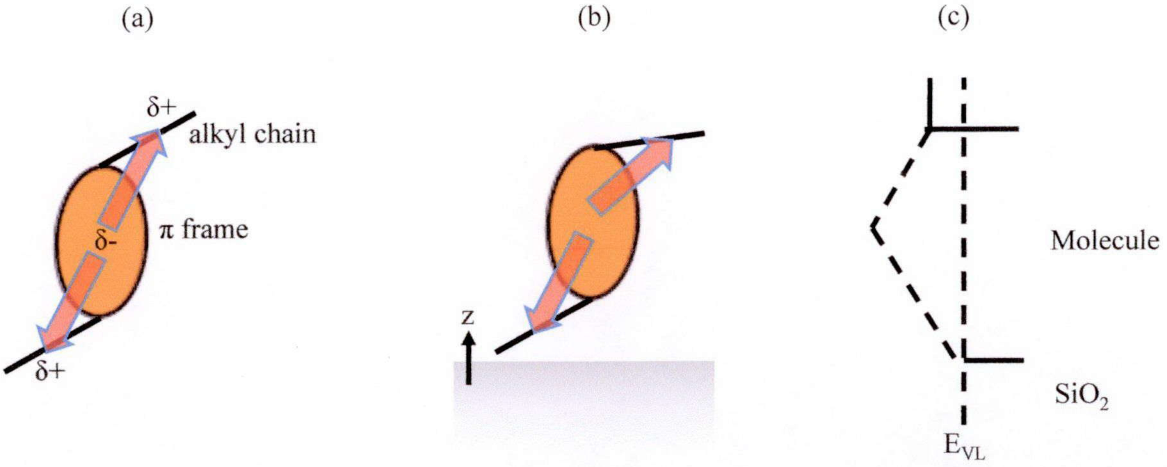

Figure 4-10. (a) Charge distribution of an isolated π-conjugated molecule with alkyl chains. (b) Deformation of the molecules by the growth on SiO_2 substrate. (c) Upper and lower dipoles induces downward and upward VL shifts, respectively. Since z component of the lower dipole is larger, the direction of a total VL shift is upward.

4-11. Electrostatic Properties of the Second Layer

The dipole induced at an OM-thick insulator interface forms the electric field. In multilayer growth, the classical electrostatics shows that the electric field propagates towards outside with decaying. This indicates that a VL shift also decays with increasing film thickness (Fig. 4-11(a)). The decay of a VL shift has been measured by PS techniques [1-3]. However, there are some exceptions that a VL shift does not follow the classical electrostatics in the multilayer (Fig. 4-11(b)) [87,88].

Duhm et al. observed the reversal from a downward VL shift to an upward VL shift with increasing thickness of PFP films on Ag(111) by using UPS [88]. They suggest that a downward VL shift of 1 ML originates from the push-back effect at a PFP-Ag interface, while an upward shift of more than 1 ML is derived from the charge transfer between the first and the upper layers. The charge transfer occurs between the energy levels modified by the structural difference: PFP molecules in the first and the upper layers grow on the Ag substrate with their molecular plane parallel and perpendicular to the surface, respectively. The electronic structure of the upper layers decreases than that of 1 ML with respect to a VL by the local dipole of C-F bond. The energy difference causes charge transfer between the first and the upper layers.

However, it remains a possibility that charge transfer occurs between the upper layer of PFP and Ag substrate, since the wave function of Ag may penetrate through the first layer. It is interesting to study the electrostatic properties of organic multilayer on SiO_2, since charge transfer between molecule and SiO_2 can be ignored. In this chapter, I fabricated 2 MLs of PEN and PFP on OH-SiO_2 and CF_3-SiO_2, and measured the VL shift by using KPFM.

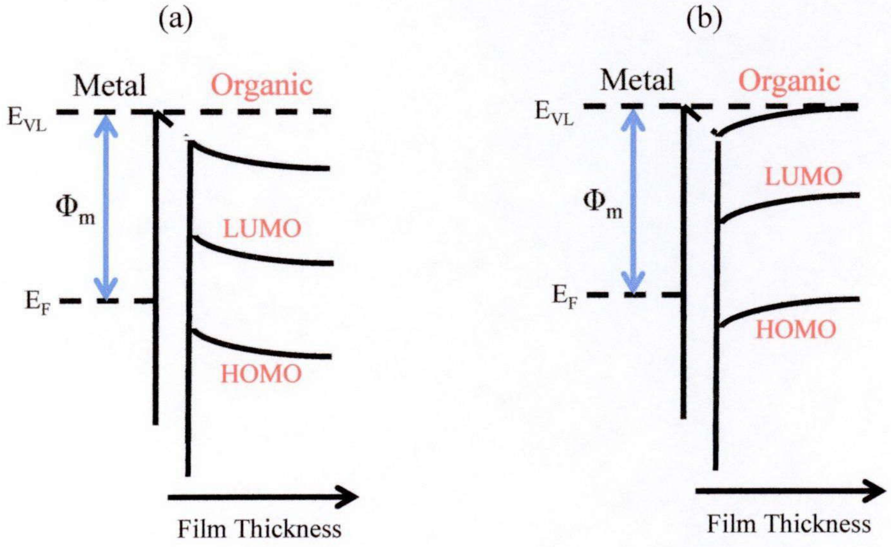

Figure 4-11. Thickness dependence of energy diagrams at O-M interfaces. (a) The dipole formed by dipole at interface propagates with thickness. (b) The direction of VL shift changes in multilayer.

4-12. Results and Discussion of Electrostatic Properties of the Second Layer

Figures 4-12(a) and 4-12(b) show the topographic images of ~1.4 ML PEN deposited on OH- and CF_3-SiO_2/Si, respectively. The dark areas reveal the first layer, while the brighter areas show the second layer. The height of the second layer with respect to the first was 1.6 nm ± 0.2 nm. The value becomes smaller than that of 1 ML. This indicates that the height difference in each layer decreases gradually with increasing film thickness and reaches the same value as that observed for the bulk crystal (1.41 nm) [82,90].

Figures 4-12(c) and 4-12(d) show the topographic images of ~1.4 ML PFP on OH- and CF_3-SiO_2, respectively. The height of the second layer was 1.5 nm ± 0.2 nm. The value also becomes smaller than that of the first. It is considered that PFP also leans at larger angle with film thickness, and the film orientation reaches the same structure as the bulk phase (1.54 nm) [82].

Figures 4-13(a) and 4-13(b) show the KPFM images of ~1.4 ML PEN on OH-SiO_2 and CF_3-SiO_2 taken simultaneously with the topographic image in Fig. 4-12(a) and 4-12(b), respectively. The second layers of PEN on both substrates appeared darker than the first layers, leading to the downward VL shift. The VL shifts of the second PEN layer with respect to the first on OH- and CF_3-SiO_2 were 90 mV and 70 mV, respectively. Figures 4-13(c) and 4-13(d) show the KPFM images of PFP on OH- and CF_3-SiO_2, respectively. The brighter contrast of the second layers for PFP revealed an upward VL shift. The VL shifts of PFP on OH- and CF_3-SiO_2 were 40 mV and 60 mV, respectively.

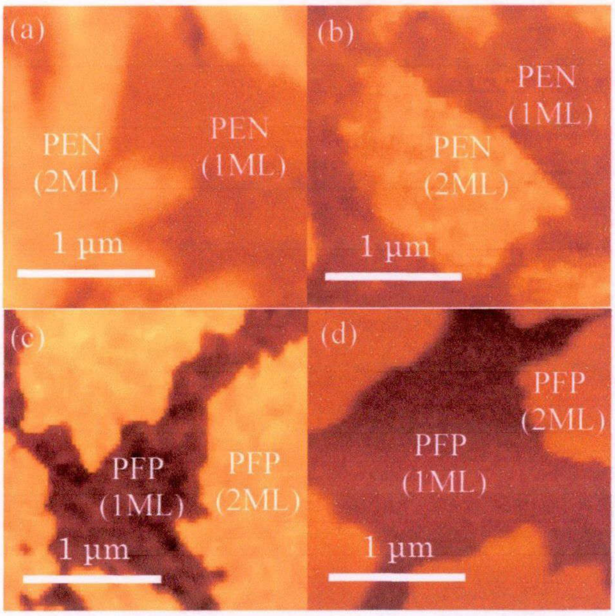

Figure 4-12. Topographic images of PEN 1.4 ML on (a) OH- and (b) F-SiO_2, and PFP 1.4 ML on (c) OH- and (d) F-SiO_2. The scan size is 2.2 µm × 2.2 µm.

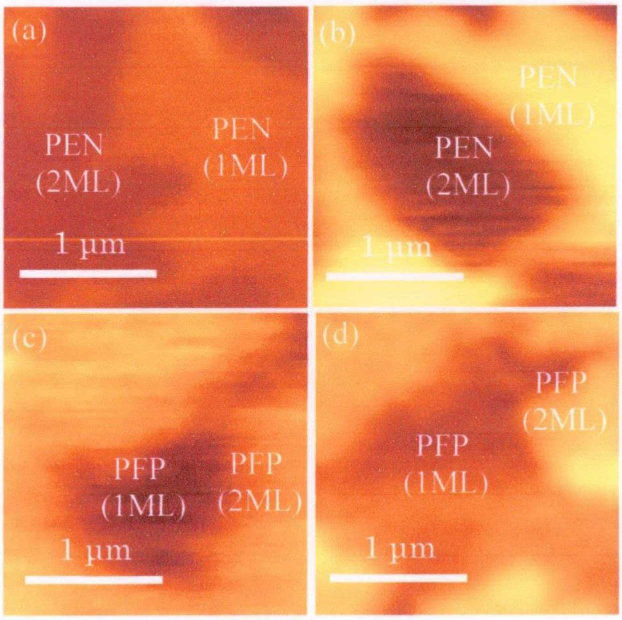

Figure 4-13. KPFM images of PEN 1.4 ML on (a) OH- and (b) F-SiO_2, and PFP 1.4 ML on (c) OH- and (d) F-SiO_2 obtained simultaneously with topographic images. The scan size is 2.2 µm × 2.2 µm.

The results are summarized as follows: the second layer of PEN on OH- and CF_3-SiO_2 showed a downward VL shift, while the second layer of PFP on OH- and CF_3-SiO_2 showed an upward VL shift. The direction of the VL shift reverses between the first and the second layers of PEN on CF_3-SiO_2 and between the first and the second layers of PFP on OH-SiO_2.

Charge transfer between the first and the second layers is one of the possibilities to determine the origin of the VL shift. The energy difference to cause charge transfer between the first and the second layers is generated by a local dipole inside molecules, ex. $C^{\delta-}$-$H^{\delta+}$ in PEN (Fig. 4-14(a)) and $C^{\delta+}$-$F^{\delta-}$ in PFP (Fig. 4-14(b)) [90]. The effect of the local dipole depends on the orientation angle of molecules in the film. According to the topographic image, PEN and PFP in the second layer tilt at a larger angle to the surface normal than those in the first layer. As a result, the energy levels of PEN and PFP in the second layer shift lower and higher than those in the first layer with respect to a VL, respectively. This indicates that charge transfer is likely to occur from the first layer to the second in PEN, causing an upward VL shift. On the other hand, PFP molecule is expected to show charge transfer from the second layer to the first, resulting in a downward VL shift. This direction of the VL shifts has conflicts with our experimental result. Thus, it is concluded that the charge transfer between the first and the second layers does not occur.

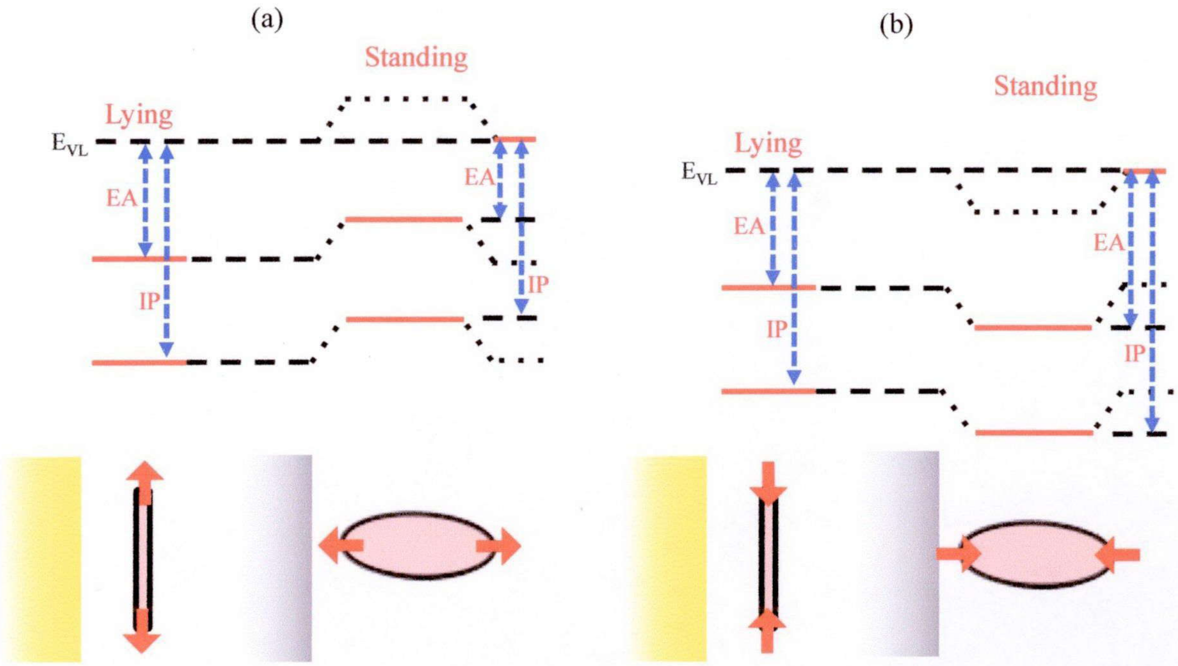

Figure 4-14. The energy levels of OMs depend on film orientation. (a) Local dipole pointed from the molecular core to the edge, such as PEN. (b) Local dipole pointed from the molecular edge to the core, such as PFP. In the former cases, the IP and EA decrease by the perpendicular orientation, while those of the latter case increase.

Hence, I extend the perspective of polarization at an OM-thick insulator interface into the multilayer. The driving force of the polarization in the second layer is considered to be dipole in π and/or σ orbital in the first layer. The former and the latter are called a π-dipole and a σ-dipole, respectively. The surface charge of the substrate induces a π-dipole in the first layer, indicating that the polarization in the second layer also may occur in the same direction. However, the VL shift of the second layer obtained is independent of the direction of a π-dipole in the first layer. On the other hand, there exists a σ-dipole generated between two atoms in molecules owing to the difference in electronegativity. In PEN, carbon and hydrogen are charged negatively and positively, respectively. The charge distribution induces the positive dipole in the π orbitals of PEN, resulting in a downward VL shift. On the other hand, a negative dipole induced by $C^{\delta+}$-$F^{\delta-}$ bond in PFP leads to an upward VL shift. This proposal agrees well with our result. The σ-dipole of molecules in the first layer determines the direction of polarization in the second layer owing to the closer distance.

Here, the electrostatic properties of more than the second layer are discussed by reference to my proposal. The polarization induced by σ-dipole depends on the structure of an underlying layer. Since the molecules is more inclined with layer thickness, the z component of the induced dipole decreases gradually. This causes the decay of the VL shift with layer thickness. After the film orientation reaches the same as that obtained in bulk crystal with further growth, the film structure does not change, indicating that a VL shift decreases at a constant value.

However, other groups [1-3,87,88] reported that the VL shift did not decrease monotonically but was saturated, when it reaches a certain thickness. Therefore, I add the effect of polarization in an underlying layer into my proposal. Figure 4-15 shows the illustration of PEN multilayer on SiO_2, where n and m are an integer number. Besides a dipole in an n+1 layer induced by σ-dipole of an n layer, the σ-dipole in an n+1 layer at the surface side is also considered to cause polarization in an n layer (Fig. 4-15(a)). The electrostatic potential of n layer consists of the dipoles induced by both n-1 and n+1 layers. The dipole direction depends on the film structure. Since molecules in an n+1 layer is more inclined than those in an n layer, z component of a dipole in an n+1 layer induced by an n layer is smaller than that in an n layer induced by an n+1 layer, indicating that the VL decays with film thickness. The dipoles in an m and an m+1 induced by each σ-dipole are cancelled out, when the film orientation reaches the same structure in bulk phase (Fig. 4-15(b)). As a result, the VL shift does not occur in the region. This improvement of the proposal is successful for explaining the saturation of the VL shift in the multilayer. The proposal can be applied to the VL shift study of PFP multilayer also. Unfortunately, it was impossible to visualize the properties of lower layer. I hope that the direct observation of the electron density in the molecule proves my proposal by other experimental techniques in near future.

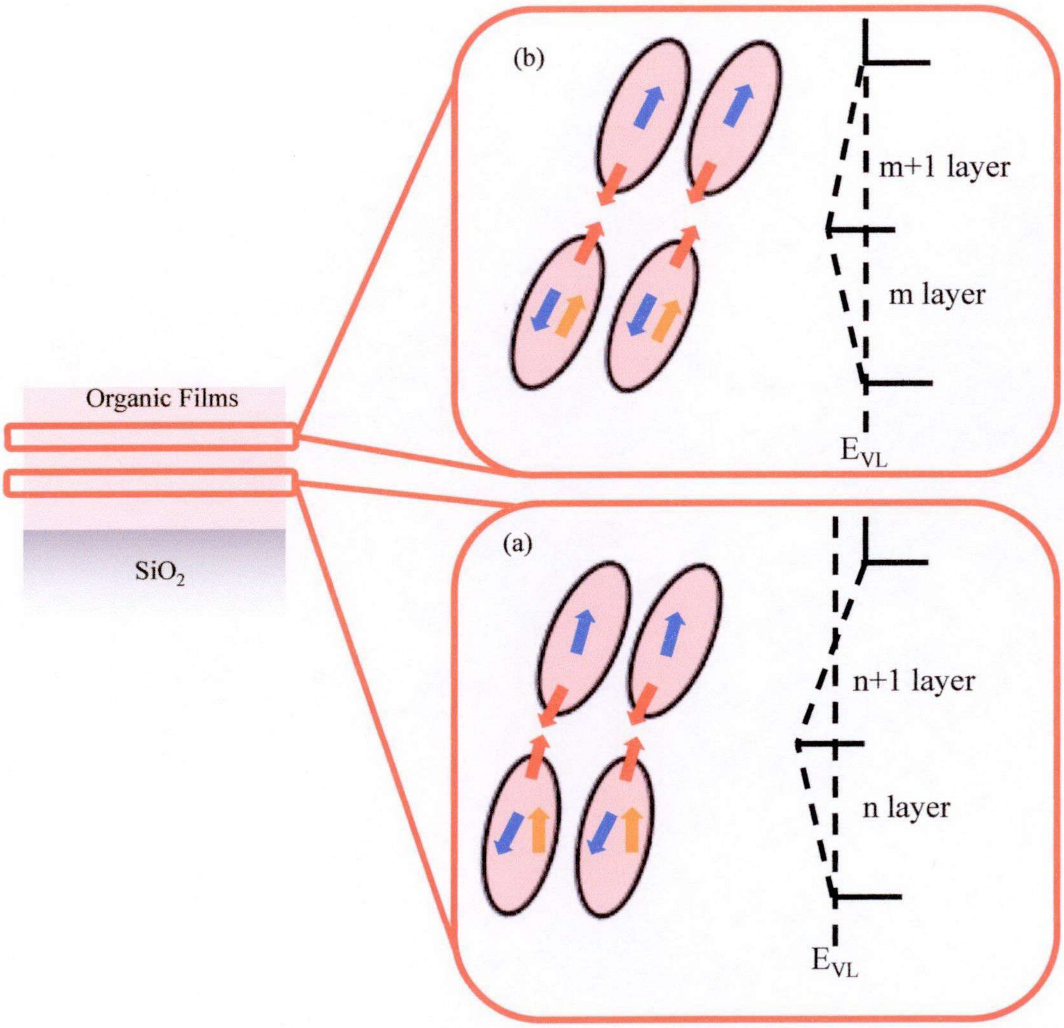

Figure 4-15. An illustration of PEN multilayer on SiO_2. Red arrows show σ-dipoles specific to molecules. Blue arrows show dipoles in an n (m) and an n+1 (m+1) layers induced by each σ-dipole. Orange arrows show a dipole in an n (m) layer induced by σ-dipole of an n-1 (m-1). Blue arrows show a dipole in an n (m) layer induced by σ-dipole of an n-1 (m-1). The energy diagram shows VL shifts induced by dipoles shown as blue arrows. (a) The structural difference in successive layers causes a VL shift. (b) Since molecular orientation does not change in the bulk phase, the induced dipoles are compensated.

Chapter 5

Geometric Dependence of Electrostatic Properties at Donor-Acceptor Interfaces

5-1. PEN-PFP Hetero-Monolayers

The mechanisms that govern interface properties of donor (D) and acceptor (A) molecules have been studied for this decade. The charge transfer between molecules has been widely accepted as the origin of the VL shift at a D-A interface on the basis of the IDIS model [26,27]. However, this model ignores the exact contact geometry at interfaces and hybridization. It is essential to clarify the geometric dependence of electronic structures at a D-A interface. In this Section, I show KPFM of the hetero-monolayer (ML) of PEN and PFP with head-to-tail and face-to-face conformations, and determine the origin of the VL shifts in each conformation.

5-2. Results and Discussion of PEN-PFP Hetero-Monolayers

5-2-1. PEN and PFP Hetero-Monolayers with a Face-to-Face Conformation

Figure 5-1(a) shows the topographic image of PEN grown on 0.4 ML of PFP pre-deposited on OH-SiO_2. In the image, there existed islands in which the outer area appeared brighter than the inner. The height of the inner area with respect to the substrate was 1.6 nm, as shown in the cross section (Fig. 5-1(c)), which is the same as that of a pure PFP film. PFP stays perpendicular to the surface. The height of an outer area was 2.0 nm. PEN is considered to construct the outer area. This film structure is acceptable in viewpoint of deposition procedure and quantities. The reason for the height difference in a hetero-ML and a pure film in our result is unclear.

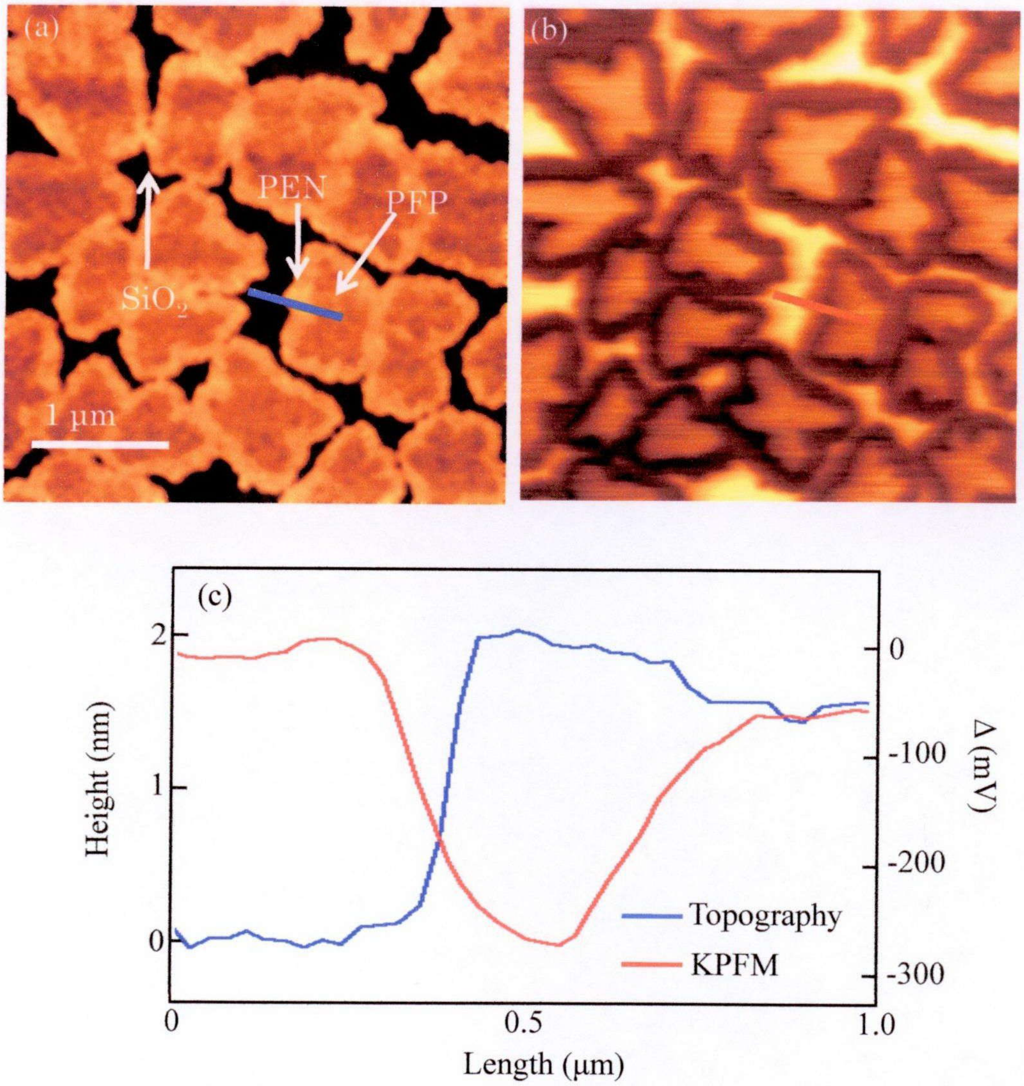

Figure 5-1. (a) A topographic image of PEN grown on 0.4 MLs of PFP pre-deposited on OH-SiO_2. (b) A KPFM image obtained simultaneously with topographic images. The scan size is 3 μm × 3 μm. (c) The height profile along the blue line in Fig. 5-1(a) and along the red line in Fig. 5-1(b).

In the formation of hetero-junction, the electrostatic interaction between two different molecules affects the contact geometry strongly. Heinderhofer et al. studied the structural properties of co-evaporated PEN and PFP on SiO_2 by using XRD measurements, and obtained the formation of 1:1 mixed films and/or the pure films according to the deposition ratio [91]. In the 1:1 mixed film, PEN and PFP were lined alternately with their molecular plane parallel to each other owing to the electrostatic force between PEN and PFP. The hydrogen of PEN is positively charged and the backbone carbon atoms are negatively charged, while the fluorine of PFP is negatively charged and the backbone carbon atoms are positively charged. The charge distribution causes the attractive forces between the backbone carbon atoms of PEN and those of PFP as well as between surrounding hydrogen of PEN and fluorine of PFP. In the hetero-ML also, the attractive force is considered to relate to the film growth. First, PEN deposited migrates on substrate and is absorbed at the edge of the PFP film. It is expected that the hetero-ML of PEN and PFP with a face-to-face conformation is formed.

Figure 5-1(c) shows the KPFM image taken simultaneously with the topographic image. The outer PEN and inner PFP films appeared darker than the substrate, indicating a downward VL shift with respect to substrate. The VL shifts of PEN and PFP were 270 mV and 60 mV, respectively (Fig. 5-1(b)).

Here, the VL shift of the hetero-ML is compared with that of pure PEN and PFP films on OH-SiO_2. The direction of the VL shift in the hetero-MLs is the same as that in PEN and PFP films deposited separately on SiO_2, indicating that a dipole in the π orbital induced by surface charges of OH-SiO_2 causes a downward VL shift. The VL shift of PEN decreases by 120 mV, while that of PFP increases by 20 mV in the formation of the hetero-MLs, as shown in Fig. 5-2(a). The energy diagram is described in Fig. 5-2(b).

Charge transfer between donor and acceptor has been widely accepted as the origin of the VL shift. The HOMO of PEN is located close to the LUMO of PFP, which causes the charge transfer from PEN to PFP. This generates the dipole at a PEN-PFP interface pointing from PFP to PEN. As a result, the VL of PFP gets higher than that of PEN. This agrees well with our result. Thus, I conclude that charge transfer is the origin of the VL shift at a D-A interface with a face-to-face conformation.

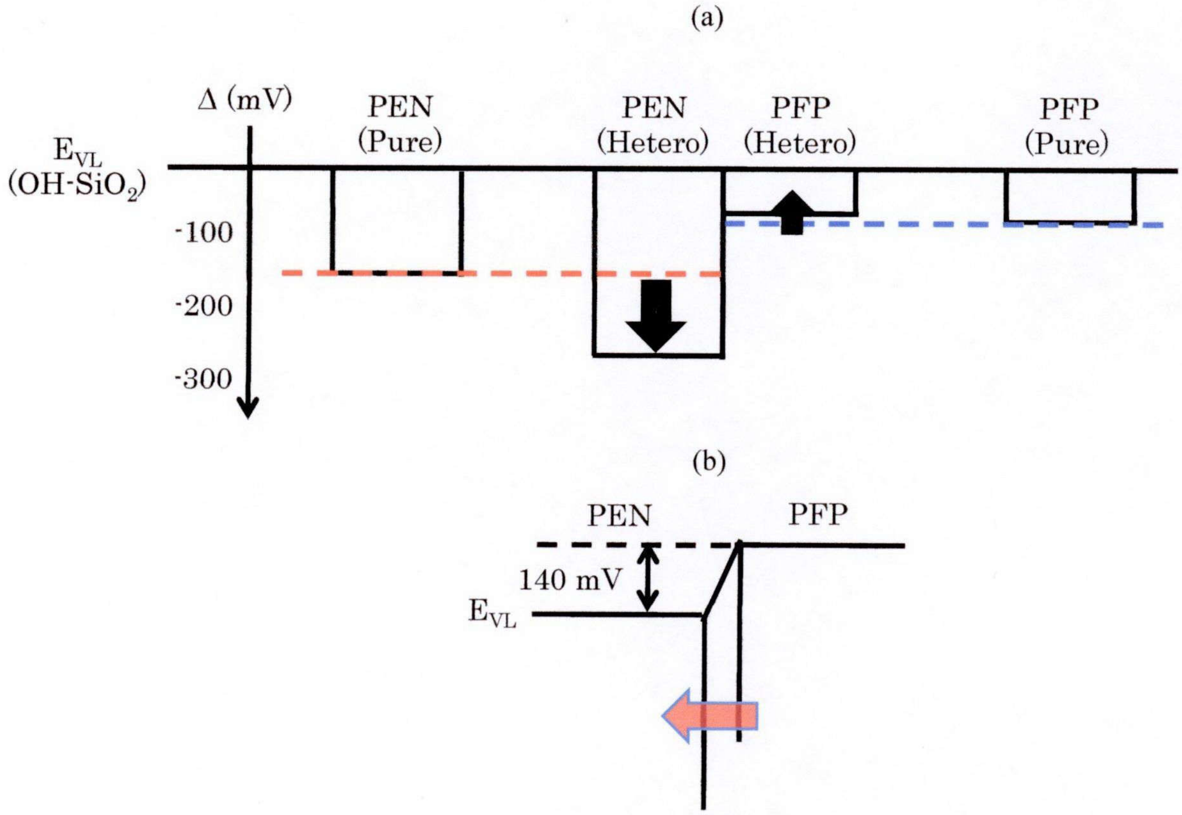

Figure 5-2. (a) VL shifts of pure films and hetero-MLs of PEN and PFP. (b) The energy level alignment at a PEN and PFP interface with face-to-face conformation.

5-2-2. PEN and PFP Hetero-Monolayers with a Head-to-tail Conformation

Figure 5-3(a) shows the topographic image of PFP grown on 0.9 ML of PEN deposited on OH-SiO$_2$. The PEN layer almost entirely covers SiO$_2$. There exists the upper layer on it. The height of the PEN layer with respect to SiO_2 is 1.8 nm, while the height of the PFP layer with respect to the PEN layer is 1.6 nm (Fig. 5-3(c)). These are the same as the height of pure PEN and PFP films. Since PFP molecules grow on a PEN film with their molecular axis approximately perpendicular to the surface, the hetero-ML is considered to form a head-to-tail conformation.

Figure 5-3(b) exhibits the KPFM image taken simultaneously with the topographic image in Fig. 5-3(a). The PEN film appeared darker than SiO_2, indicating a downward VL shift. The darker contrast of the PFP layer also represents a downward VL shift with respect to a lower PEN layer. The VL shift of PEN was 150 mV, while the VL shift of PFP was 100 mV (Fig. 5-3(c)).

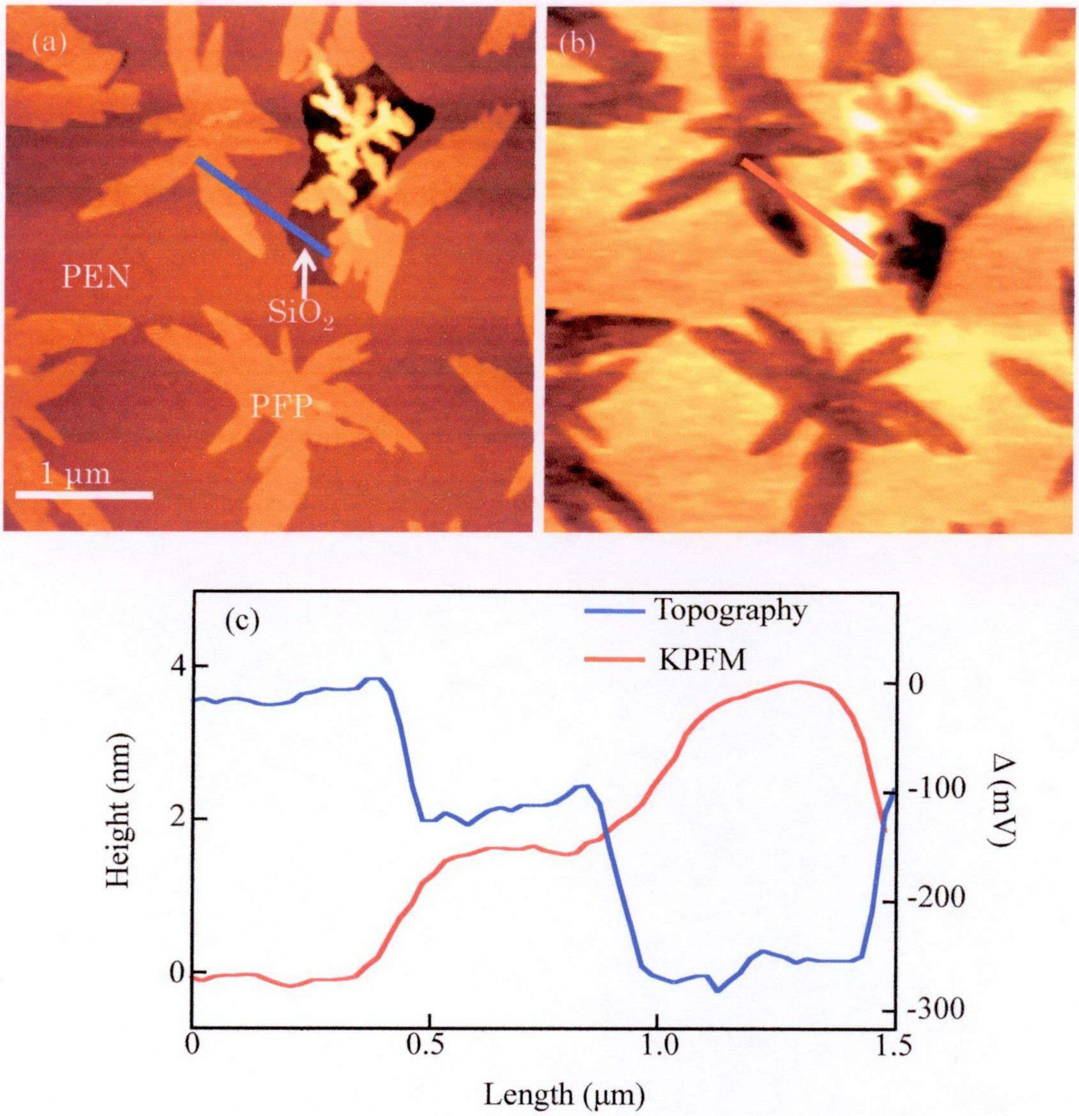

Figure 5-3. (a) A topographic image of PFP grown on 0.9 MLs of PEN pre-deposited on OH-SiO_2. (b) A KPFM image obtained simultaneously with topographic images. The scan size is 3 μm × 3 μm. (c) The height profile along the blue line in Fig. 5-1(a) and along the red line in Fig. 5-1(b)

The VL shift of a lower PEN layer remains unchanged in the growth of the PFP layer. The direction of the VL shift of PFP/PEN is opposite to that of a face-to-face conformation. If the VL shift of the PFP/PEN also originates from charge transfer, the downward VL shift of PFP/PEN predicts that PFP donates electrons to PEN. However, this is unlikely to occur, since the HOMO of PEN and the LUMO of PFP is located at the same energy level. The discrepancy is considered to attribute to the contact of σ orbital in head-to-tail conformation, which avoids the hybridization between π orbital. This indicates that the IDIS model is beyond the limits of validity, when the hybridization between π orbital is weak.

Hence, I focus on the effect of polarization in order to determine the origin of the VL shift in head-to-tail conformation. In a CH group of PEN, carbon and hydrogen are charged negatively and positively, respectively owing to the difference in electronegativity. This charge distribution induces a positive dipole in PFP on PEN. This agrees well with our results. Thus, it is concluded that the origin of the VL shift in a head-to-tail conformation is a dipole induced by charge of a lower layer. The energy diagram is described in Fig. 5-4.

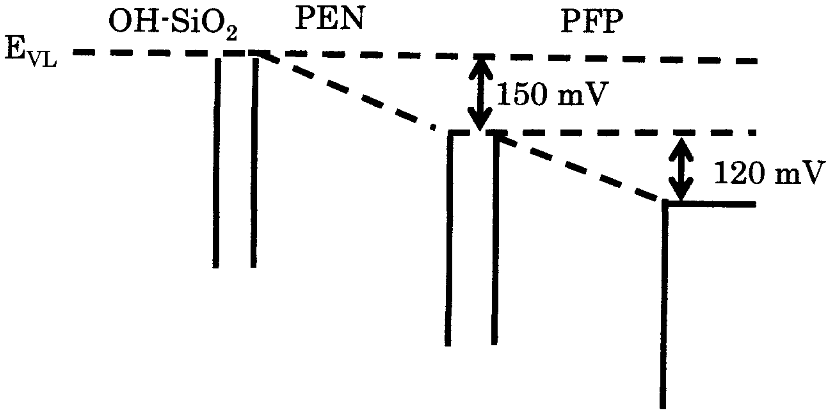

Figure 5-4. The energy diagram of PFP on PEN grown on OH-SiO_2.

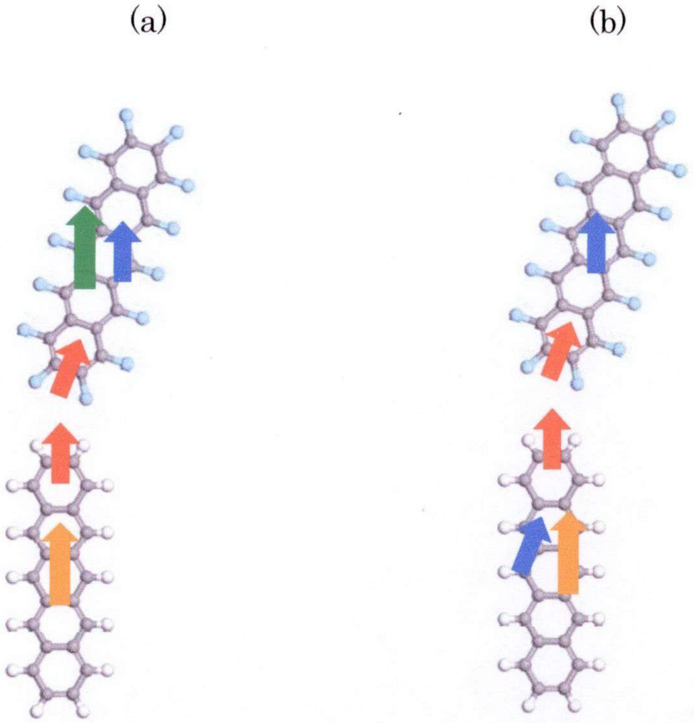

Figure 5-5. (a) An illustration of a π-dipole (green and blue arrows) in PFP induced by a σ-dipole (red) of PEN and a π-dipole (orange) in PEN induced by the surface charge of SiO_2. (b) An illustration of a π-dipole (blue) in PFP induced by a σ-dipole (red) of PEN, and a π-dipole (blue) in PEN induced by a σ-dipole (red) of PFP.

A VL shift depends on surface charges and/or dipole of chemical species. Since a dipole of CH group is smaller than that of OH-group, the induced dipole of PFP on PEN is considered to be smaller than that of PFP on OH-SiO_2. However, the VL shift of PFP on PEN observed was larger than that of PFP on OH-SiO_2. There are two possibilities to explain a large VL shift. One of the possibilities is that not only a positive σ-dipole of CH bond but also a positive π-dipole in PEN affects the polarization of PFP (Fig. 5-5(a)). Both effects induce a larger dipole in PFP. Another possibility is that a π-dipole in PEN is induced by C-F bond of a PFP layer (Fig. 5-5(b)). In a fluorocarbon group of PFP, carbon and fluorine are charged positively and negatively, respectively. The charge distribution of PFP induces the positive π-dipole of PEN. Both positive π-dipole of PEN and PFP makes the VL shift of

PFP/PEN larger than that of PFP/OH-SiO_2. These two proposals are considered to be suitable for the origin of a larger VL shift of PFP/PEN, although it is difficult to determine which factor is more dominant.

5-2-3. Summaries

The results are summarized as follows: At the interface with a face-to-face conformation, the origin of VL shift is an electron transfer from PEN to PFP. The VL shift of the D-A interface with a head-to-tail conformation originates from a dipole induced by a local dipole on the surface of lower layer. This supports the theoretical approach reported previously [28-30]. The authors revealed that a dipole at a D-A interface is governed by a partial charge transfer between donor and acceptor units as well as by a mutual polarization of the electric clouds according to the strength of the hybridization of π orbitals.

Our proposal has a conflict with the previous experimental reports. The UPS of CuPc and F16CuPc hetero-layer suggested that charge transfer occurs not only in face-to-face conformation but also in a head-to-tail conformation [31]. In addition, they proposed that charge transfer in the head-to-tail conformation was larger than that of the face-to-face. This is attributed to the large energy difference between CuPc and F16CuPc in the head-to-tail conformation, since the energy level is modified by the local dipole owing to the perpendicular orientation on the substrate, as shown in Fig. Fig. 4-13.

Duhm et al. studied the electronic structure of the head-to-tail conformation of PEN and PFP on SiO_2 [32]. They showed no shift of the energy levels owing to weak hybridization between σ orbitals. This is similar to my experimental result. However, the polarization effect is not observed. They grow molecular layers on 3-nm-thick films of the other molecules pre-deposited on SiO_2. 3-nm-thick PEN or PFP corresponds to two or three layers with pyramid-like structure [75,92]. The PEN deposited is considered to adsorb at the edge of the multilayer of PFP, causing the formation of the face-to-face conformation, and vice versa. As a result, the VL shift obtained by UPS is composed not only of polarization but also of charge transfer. It is found that their preparation of a head-to-tail conformation is incomplete. On the other hand, it is evident that my sample consists of only the head-to-tail conformation from the topographic image. Thus, the preparation of the well-defined hetero-MLs with face-to-face and head-to-tail conformations demonstrates that charge transfer and polarization determine the VL shift at a D-A interface with the displacement of each π orbital.

5-3. PEN-PFP Hetero-Multilayers

The KPFM studies of a PEN and PFP hetero-ML have revealed that the electrostatic properties at a D-A interface correlated highly with the film structures and hybridization. The origins of VL shift in head-to-tail and face-to-face conformations were induced dipole and charge transfer, respectively. This is the extremely simple case. The hetero-multilayer in an actual device consists of various interface structures. As shown in Duhm's report [32], the formation of a hetero-multilayer makes the interfacial properties complicated. It is essential to study the relation between the contact geometry and the electronic structures in the hetero-multilayer. In this Section, I prepared the hetero-multilayer of PEN on pre-deposited PFP on SiO_2, and investigated the electrostatic properties by using KPFM. The coverage of PFP pre-deposited on SiO_2 was estimated to be 1.1 ML. The deposition quantity of PEN was approximately the fourth of that in PEN/PFP hetero-MLs, which was estimated by the frequency shifts measured by quartz oscillator.

5-4. Results and Discussion of PEN and PFP Hetero-Multilayers

5-4-1. Topographic information of PEN and PFP Hetero-multilayers

Figure 5-7(a) shows the topographic image of PEN grown on PFP covered on SiO_2. There appeared various areas in the film assigned ② - ⑦. The darkest area ① is SiO_2. These are named areas ② - ⑦, respectively. From the height analysis, the structural properties of these areas are easily distinguished, except for areas ③ and ④. The height of area ② with respect to SiO_2 is 1.6 nm. Since this is the same height as pure PFP film, it is considered that the area ② consists of PFP. The areas ⑤-⑦ are grown on the underlying PFP layer (②). The height of areas ⑤ and ⑥ with respect to the lower layer is 1.6 nm, and that of area ⑦ is 1.5 nm. Since these heights are similar to those of 2 ML in PEN and PFP, the areas ⑤ and ⑥, and ⑦ are considered to be PEN and PFP films, respectively. Therefore, the area ⑤ corresponds to PEN/PFP hetero-layer with head-to-tail conformation. Additionally, the areas ⑥ and ⑦ are also considered to show the hetero-layer with face-to-face conformation at the interface due to an attractive force, such as PEN/PFP on SiO_2.

The areas ③ and ④ are formed at the edge of area ② and inside the area ②, respectively. The heights of areas ③ and ④ with respect to SiO_2 are 1.8 nm, which indicates that the areas are considered to consist of PEN from the height. However, the AFM observation indicated that the first layer was almost completely covered on SiO_2 and the second layer was grown on it, when a PFP film was prepared with the same condition. There existed a few SiO_2 areas below the size of 50 nm × 50 nm in a scan range of 10 μm × 10 μm, which means little room of the growth in PEN. It is considered that PEN is unlikely to grow at the edge of and inside PFP films. I propose that the thermal diffusion of PEN causes the mixing of PEN and PFP. Hinderhofer et al. showed the formation of the pure and 1:1 mixed film in co-deposition of PEN and PFP by using X-ray diffraction technique [91]. The mixed film with the other ratios was not observed. It is also expected that the areas ③ and ④ are the 1:1 mixed film in my experiment.

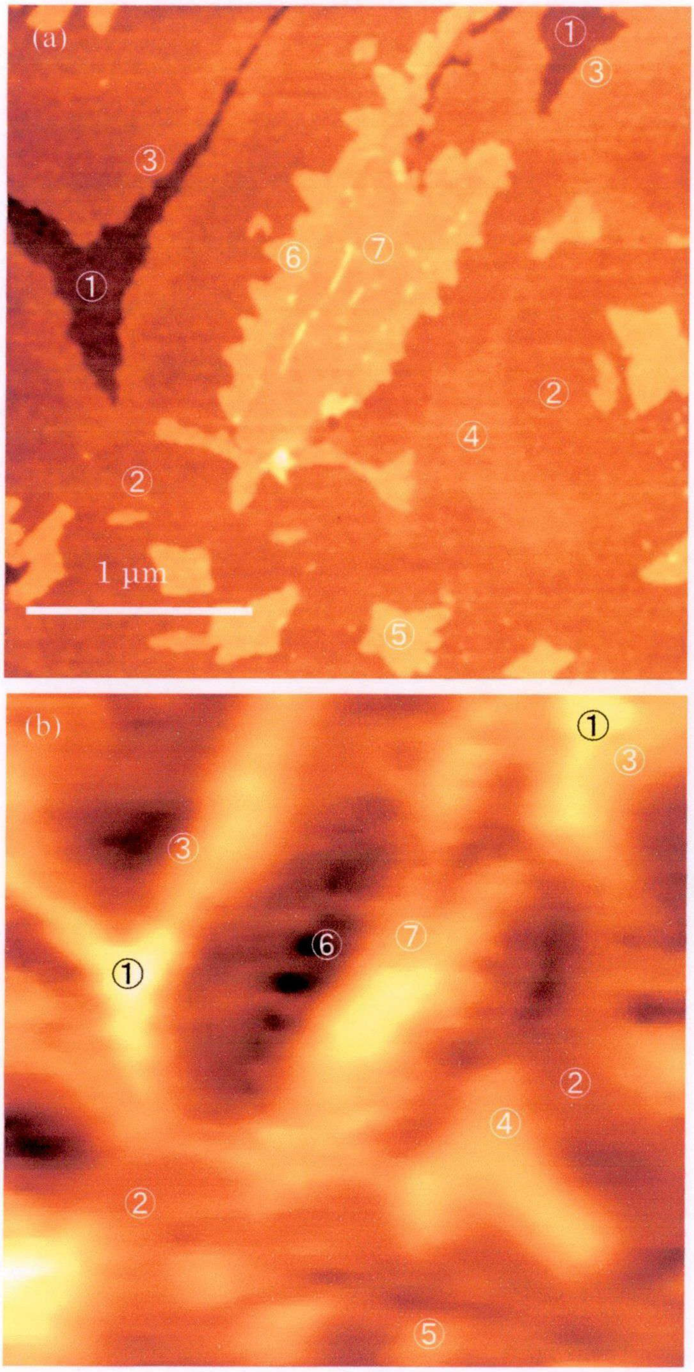

Figure 5-7. (a) A topographic image of PEN grown on 1.1 ML of PFP covered on SiO_2. (b) A KPFM image obtained simultaneously with topographic images. The scan size is 3 µm × 3 µm.

5-4-2. KPFM information of PEN and PFP Hetero-Multilayers

Figure 5-7(b) shows the KPFM image obtained simultaneously in the topographic image (Fig. 5-7(a)). The KPFM results are shown in Table 5-1.

Table 5-1. The KPFM results obtained in a PEN-PFP hetero-multilayer.

Area	Film structure	Δ (mV) with respect of [Materials]
①	SiO_2	-
②	PFP 1 ML	-80 [SiO_2]
③	A mixed layer at the edge of PFP 1 ML	-10 [SiO_2]
④	A mixed layers inside PFP 1 ML	-10 [SiO_2]
⑤	PEN/PFP 1 ML	+40 [PFP 1 ML]
⑥	PEN in a hetero-layer/PFP 1 ML	-30 [PFP 1 ML]
⑦	PFP in a hetero-layer/PFP 1 ML	+80 [PFP 1 ML]

First, the KPFM of hetero-layer with a well-defined conformation (②, ⑤-⑦) is discussed. In the KPFM image, the underlying PFP layers in ② appeared darker than SiO_2, indicating a downward VL shift. The VL shift of area ② is 80 mV. The downward VL shift in the area ② is considered to originate to a dipole in PFP induced by the surface charge of OH-SiO_2. The VL shift of 80 mV is the same as that of PFP film on OH-SiO_2, indicating little charge transfer between ② and ③ (④).

In the image, the area ⑤ appeared brighter than the first PFP layer, indicating an upward VL shift. The VL shift is 40 mV. The areas ⑥ and ⑦ appeared darker and brighter than the lower layer, resulting in that the areas ⑥ and ⑦ reveal downward and upward VL shifts, respectively. The VL shifts of ⑥ and ⑦ are 30 mV and 80 mV, respectively. The origin of the VL shift at a head-to-tail D-A interface was a dipole in molecules induced by surface charges of the first PFP layer, as proposed in Sec. 5-2. The carbon and fluorine atoms in PFP are charged positively and negatively, respectively. The charge distribution of the first layer induces a negative dipole in PEN (⑤), leading to an upward VL shift. This agrees well with our experiment. It is found that charge transfer and/or polarization determine the origin of VL shift for a hetero-junction with a well-defined contact geometry. The areas ⑥ and ⑦ form a face-to-face hetero-ML on PFP layers. The component of a PEN and PFP interface is taken out, in comparison with the VL shift of pure films. The VL shift of area ⑥ decreases by 70 mV than that of PEN/PFP (⑤), while the VL shift of area ⑦ increases by 40 mV than that of 2 ML of PFP. Based on the result, the energy level is described in Fig. 5-8. The direction of the VL shift at the PEN-PFP interface coincides with that obtained by charge transfer from donor to acceptor. It is found that the origin of the VL shifts at the interface between areas ⑥ and ⑦ is also charge transfer owing to the hybridization between each π orbital.

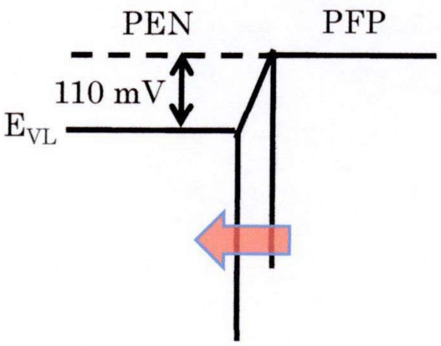

Figure 5-8. The energy diagram of PFP-PEN hetero-layers grown on a PFP ML.

Next, the properties of the mixed layer (③ and ④) are examined. The area ③ and ④ showed a downward VL shift of 10 mV, which was larger than those of PEN and PFP film deposited on SiO_2 separately. This indicates that the VL shift originates not only from polarization but also from the other factor. One of the possibilities for the factor is charge redistribution. Since PEN is faced to PFP in the mixed film, charge transfer is considered to occur from PEN to PFP, which may cause charge redistribution inside the mixed film. However, there is no evidence, since the properties inside a mixed layer is not observed. Actually, I fabricated the mixed film of PEN and PFP deposited simultaneously on SiO_2 at the substrate temperature of 80 ℃, as reference to Hinderhofer's report [91]. The KPFM of co-deposited PEN and PFP showed a downward VL shift of 10 mV. This coincides with the result of areas ③ and ④.

These results indicate that the VL shifts at the well-defined D-A interfaces can be determined by charge transfer and polarization with the contact geometry. However, a further deposition is associated with a high possibility of an unexpected mixing. Since actual organic devices are prepared in the successive multilayer with several tens of nm, it is considered that many mixed films are formed at the interface. I hope that the electrostatic properties of the mixed film are measured with a single molecular level by the combination of KPFM with NC-AFM in near future.

5-5. Oligothiophene and PFP Hetero-Monolayers

5-5-1. Oligothiophene and PFP Hetero-Monolayers with A Face-to-face Conformation

The KPFM of hetero-ML of PEN and PFP suggests that a VL shift at a D-A interface is sensitive to a contact geometry. Charge transfer occurs from a donor to an acceptor when their π orbital is close to each other. In this Section, I show the KPFM of hetero-MLs with n-thiophene (5T, 6T and 7T) and PFP on SiO_2, and clarify the effect of a partial hybridization on VL shifts.

5-5-2. Results and Discussion of Oligothiophene and PFP Hetero-Monolayers with a Face-to-face Conformation

Figure 5-9(a) shows the topographic image of PFP on 6T films pre-deposited on OH-SiO_2. There are islands with two areas. The height of inner film with respect to SiO_2 is 2.7 nm, and that of outer film is 1.6 nm. The inner and outer films are considered to be 6T and PFP, respectively. Both molecules grow on SiO_2 with their long axes perpendicular to the surface. The geometric structure at the interface cannot be observed in my measurement. 6T consists of the negatively charged carbon and the positively charged hydrogen and sulfur atoms, while PFP has the negatively charged fluorine and positively charged carbon. It is presumed that the molecular plane of 6T faces that of PFP owing to the attractive force, such as a PEN-PFP system.

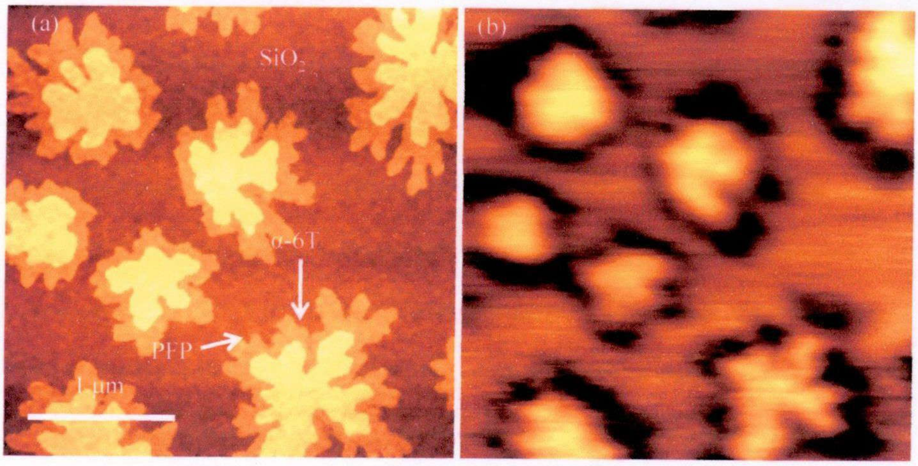

Figure 5-9. (a) Topographic and KPFM images of a PFP-6T hetero-ML on SiO_2. The scan size is 3 μm × 3 μm.

Figure 5-9(b) shows the KPFM of 6T and PFP hetero-junction on SiO_2 obtained simultaneously with the topographic image in Fig. 5-3(a). The 6T and PFP films appeared brighter and darker than OH-SiO_2, indicating upward and downward VL shifts, respectively. The VL shift of α-6T was 120 mV and that of PFP was 70 mV.

The VL shift of the face-to-face hetero-ML is compared with that of the 6T and PFP film on SiO_2 deposited separately on SiO_2. The direction of the VL shift of PFP in the hetero-ML is the same as that in the PFP film on SiO_2, indicating that a dipole is induced by the surface charge of OH-SiO_2. The VL shift of 6T in a hetero-ML is larger than that in a pure film. On the other hand, 6T shows the change from an upward to a downward VL shift by the formation of a hetero-ML. Therefore, a dipole is induced by the surface charge is not the origin of VL shift for 6T in a hetero-ML.

In Sec. 4-2, it is proposed that charge transfer occurs between donor and acceptor, when each π orbital is closer. Since the HOMO of 6T is located close to the LUMO of PFP, the charge transfer occurs from 6T to PFP. The hybridization of π orbital is limited up to the height of PFP, since 6T is longer than PFP. As a result, the electron of a lower part in 6T is transferred into the PFP. This generates a dipole in 6T pointing from the lower to the upper part, indicating an upward VL shift. On the other hand, PFP is negatively charged in the whole area, resulting in the increase in the VL shift. This speculation agrees well with my result.

I calculated the electronic structure of 6T and PFP dimer by DMol3, in order to support the proposal. The dimer of 6T and PFP has a cofacial structure. The energy diagrams of isolated molecule and dimer of 6T and PFP are shown in Fig. 5-10(a). The HOMO level of dimer contributes to the upper parts of 6T (Fig. 5-10(b)), while the LUMO level originates from the lower parts of n-thiophene and PFP (Fig. 5-10(c)). It clearly presents the electron transfer from a lower part of 6T to PFP. The calculation result supports our proposal. It is concluded that the charge distribution of a longer molecule induced by a partial charge transfer determines a VL shift of face-to-face hetero-ML of molecules with different height.

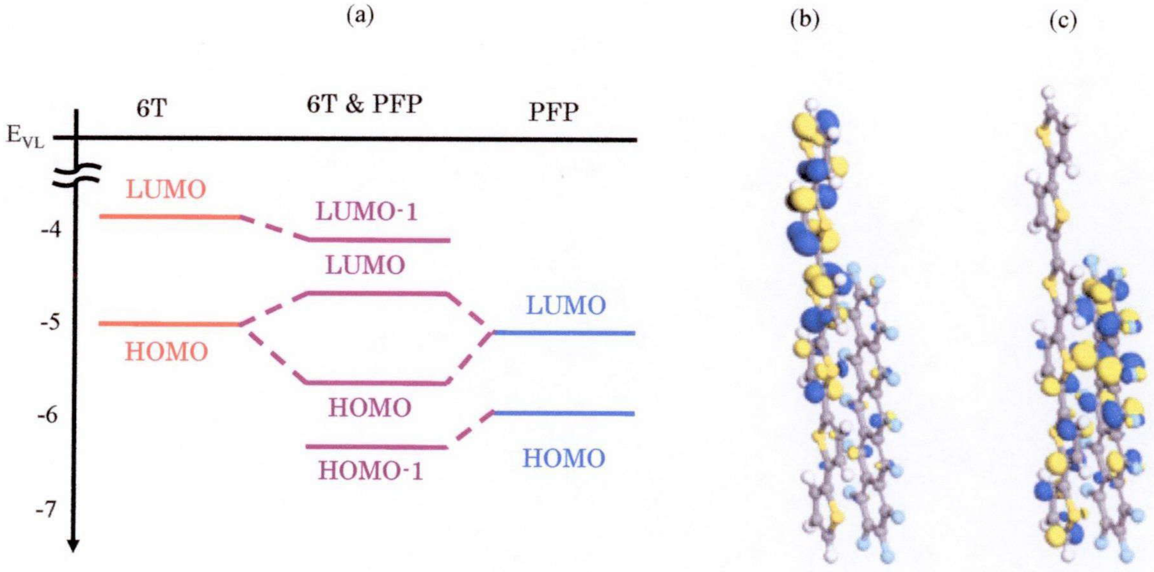

Figure 5-10. (a) Energy diagram of isolated 6T and PFP molecules, and the dimer. The molecular orbitals of (b) HOMO and (c) LUMO levels in the dimer.

Figures 5-11(a) and 5-11(b) show the topographic image of PFP films on 5T and 7T pre-deposited on SiO_2, respectively. In these films, there are islands with two areas. The inner and outer films are considered to be n-thiophene and PFP, respectively. Since the attractive force acts between n-thiophene and PPF, it is also presumed that the face-to-face conformation is formed at the interface.

Figures 5-11(c) and 5-11(d) show the KPFM images of 5T-PFP, and 7T-PFP hetero-junctions on SiO_2, respectively. The n-thiophene and PFP films appeared brighter and darker than OH-SiO_2, indicating upward and downward VL shifts, respectively. Therefore, the partial charge transfer as well as the polarization is considered to determine the VL shift. The VLs of 5T-PFP and 7T-PFP hetero-MLs are arranged in Fig. 5-12, by adding the result of a 6T-PFP hetero-ML. The VL shifts of n-thiophene and PFP increase along with number of a thiophene ring.

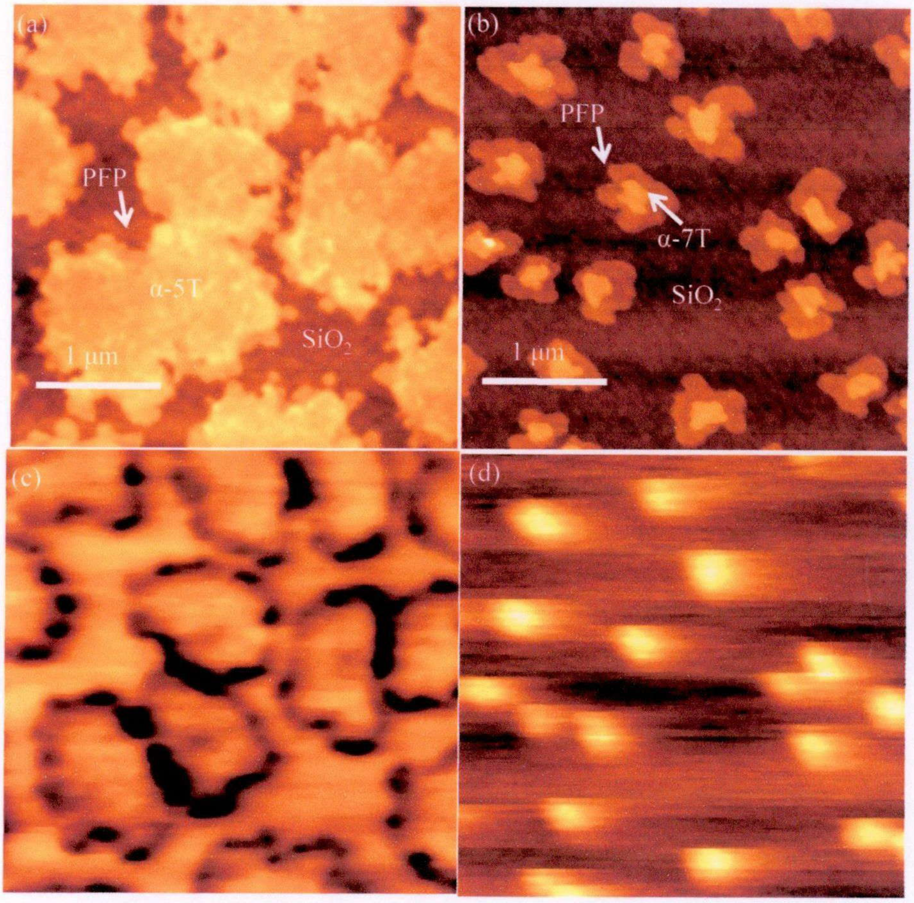

Figure 5-11. Topographic images of (a) PFP-5T and (b) PFP-7T hetero-MLs on SiO_2. The KPFM images of (c) PFP-5T and (c) PFP-7T hetero-MLs on SiO_2 obtained with the topographic images. The scan size is 3 μm × 3 μm.

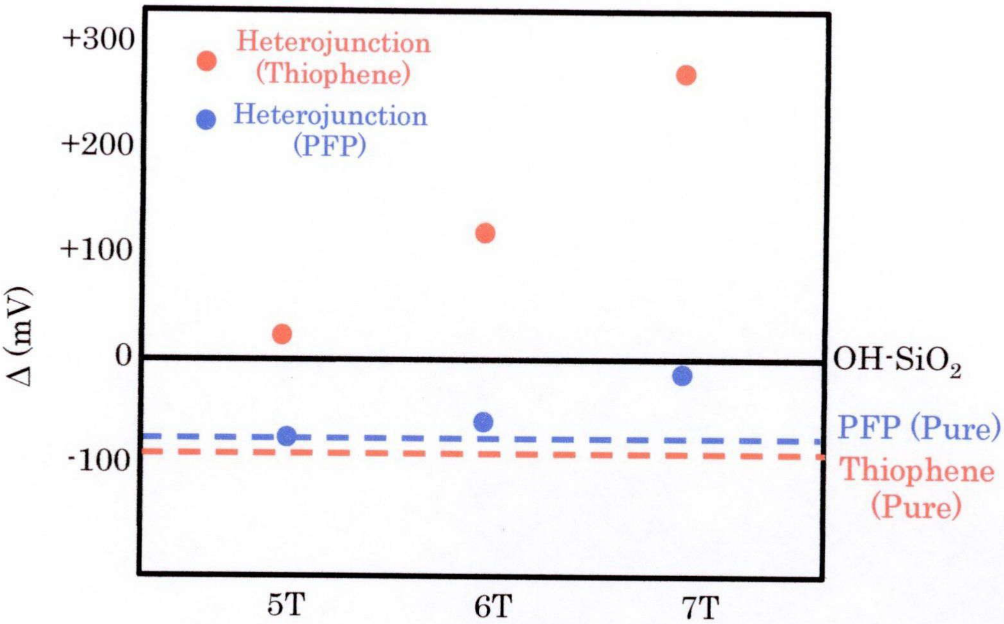

Figure 5-12. The VL shifts of pure films and hetero-MLs in 5T, 6T and 7T.

The KPFM of 5T-PFP, and 7T-PFP hetero-MLs also indicates the partial charge transfer from n-thiophene to PFP. The charge transfer depends on the energy level position. Since the energy difference between the HOMO of n-thiophene and the LUMO of PFP (Fig. 5-13), charge transfer is considered to become larger with the molecular length. As a result, PFP is more negatively charged with ring number of n-thiophene, which causes the increase in the VL shifts. The lower part of n-thiophene is also more positively charged with molecular length, indicating a larger dipole in n-thiophene. In addition, the molecular length affects the dipole, since a dipole is expressed as the multiplication of charge and length. Therefore, the increase in VL shifts of n-thiophene is considered to be larger than that of PFP. This coincides with my result. In this Section, I demonstrate the length dependence of the VL shift at an n-thiophene and PFP interface.

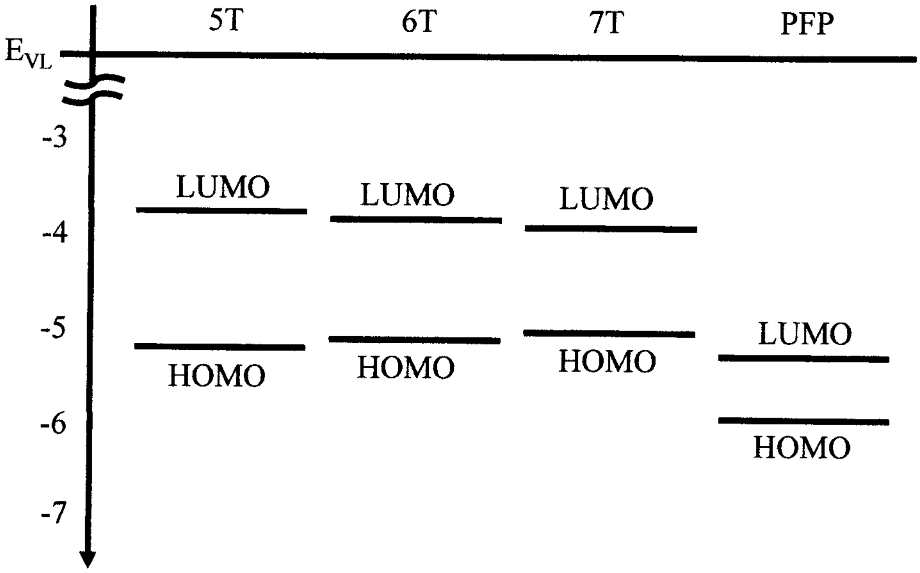

Figure 5-13. Energy diagrams of 5T, 6T, 7T and PFP.

5-5-3. Oligothiophene and PFP Hetero-Monolayers with a Head-to-tail Conformation

In Sec. 5-2, I proposed that the direction of a VL shift at a D-A interface with a head-to-tail conformation originates to the polarization in π orbital. It is difficult to determine the magnitude of a VL shift. The KPFM of PFP on PEN suggests that a dipole in π orbital of the charge distribution of the layer induces a dipole in the underlying layer, and/or the polarization in π orbital of the underlying layer affects the upper layer. In this Section, I prepared the head-to-tail junction of PFP/6T surrounded of PFP, and measured the electrostatic properties by KPFM. In the preparation, the twice deposition of PFP speed is needed.

5-5-4. Results and Discussion of Oligothiophene and PFP Hetero-Monolayers with a Head-to-tail Conformation

Figure 5-14(a) shows the topographic image of PFP on 6T film pre-deposited on

SiO_2. Besides the formation of the hetero-ML of α-6T surrounded by PFP, there appeared the PFP layers on 6T layers. The height of the upper layer with respect to α-6T film is 1.5 nm, indicating that PFP tilts by 25 degree to the surface normal.

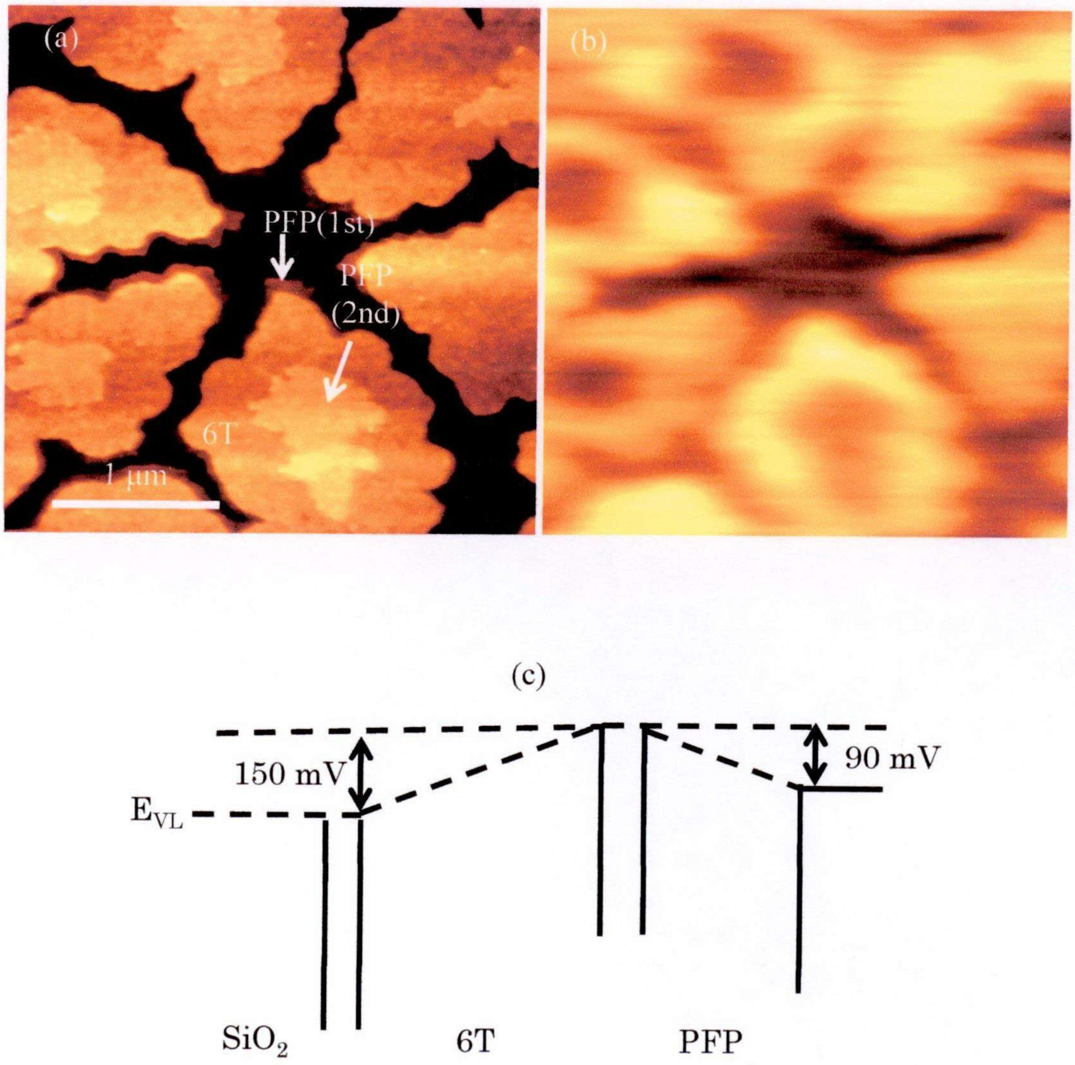

Figure 5-14. (a) A topographic image of the PFP ML on the 6T-PFP hetero-ML grown on OH-SiO_2. (b) A KPFM image obtained simultaneously with topographic images. The scan size is 3 μm × 3 μm. (c) The energy diagram of PFP on 6T grown on OH-SiO_2.

Figure 5-14(b) shows the KPFM image taken simultaneously with the topographic image. 6T layers were brighter and surrounding PFP layers were darker than SiO_2. The PFP film on 6T appears darker than the underlying layer, indicating a downward VL shift. The VL shifts of 6T, surrounding PFP and upper PFP layers are 120 mV, 70 mV and 90 mV, respectively. The VL shifts of 6T and surrounding PFP films did not change in growth of upper PFP layer.

The origin of the VL shift at a D-A interface with head-to-tail conformation is a dipole in molecules induced by charge distribution. Since the hydrogen and carbon atoms of 6T are positively and negatively charged, respectively, the positive dipole is induced in PFP, causing the downward VL shift. Thus, the energy diagram can be described, as shown in Fig. 5-14(c). The VL shift of PFP on 6T is larger than that of PFP on OH-SiO_2, although the dipole of OH group is larger than that of CH group. It is proposed that a π-dipole of an underlying layer is induced by σ-dipole of an upper layer and/or the π-dipole in an underlying layer affects an upper layer. Since the direction of a π-dipole in 6T of a hetero-ML is the opposite to a dipole induced in PFP upper layer, the VL shift is not determined by the dipole in π orbital of an underlying layer. This suggests that the effect of the π-dipole in both layers induced by each σ-dipole determines the VL shift at a D-A interface with a head-to-tail conformation.

Chapter 6

Conclusions and Outlook

This work focused on the investigation by means of KPFM of monolayers (MLs) and hetero-layers of plate-like and alkylated plate-like conjugated molecules grown on SiO_2 substrates. These molecules grew on SiO_2 with the long axes perpendicular to the surface. The KPFM results determined the origin of VL shifts at O-I and O-O interfaces in Chapter 4 and 5, respectively.

In Sec. 4-2, 4-4 and 4-6, the origin of a VL shift at a plate-like OM-thick insulator is clarified through KPFM studies on organic MLs grown on 300-nm-thick thermal SiO_2. The KPFM of PEN on thermal SiO_2/p-Si and n-Si presents the same VL shift. This indicates that the energy level of background Si does not affect the VL shift, since a thick insulator avoids charge transfer between them. The PEN and PFP MLs deposited on OH- and CH_3-SiO_2 showed a downward VL shift, while those on CF_3-SiO_2 showed an upward VL shift. It is suggested that the VL shift at a plate-like OM-thick insulator originate not from the charge transfer but from the dipole induced in π orbital of molecules by surface charges.

In Sec. 4-8, the KPFM of 5T, 6T and 7T MLs on OH-SiO_2 have carried out to study the length dependence of VL shift. All of three thiophene MLs exhibits the downward VL shifts of 90 mV. These are also considered to derive from a dipole induced by the surface charge. The relation between polarizability and relative dielectric constant is estimated on the basis of Helmholtz equation. It represents that the polarizability of n-thiophene increases with ring number in proportion to the relative dielectric constant.

In Sec. 4-10, the effect of alkyl chain with VL shift is examined by means of KPFM of DH-6T and PTCDI-C13 MLs on OH-SiO_2. DH-6T and PTCDI-C13 shows upward VL shifts, in contrast with plate-like molecules on OH-SiO_2. It indicates that the alkyl chains between the π-system and SiO_2 reduce the effect of surface charges. The structural asymmetry of these molecules causes the VL shift.

In Sec. 4-12, the electrostatic properties of PEN and PFP 2 ML have been studied from their VL shifts obtained by KPFM. PEN 2 MLs on OH- and F-SiO_2 show a downward VL shift with respect to 1 ML, while PFP 2 MLs on OH- and F-SiO_2 show an upward VL shift. Thus, the direction of the VL shift of 2 ML is considered to originate from the surface charges of 1 ML.

In Sec. 5-2, KPFM of PEN and PFP hetero-MLs with face-to-face and head-to-tail conformations have carried out. The deposition of PEN on PFP/SiO_2 exhibits a hetero-ML with a face-to-face conformation at the interface. The VL shift of PEN of PFP becomes smaller and larger, respectively, by the growth of the face-to-face hetero-MLs, in comparison with each pure film. It is found that the VL shift of a face-to-face hetero-ML originates in a charge transfer from PEN to PFP. On the other hand, the head-to-tail conformation is formed by the deposition of PFP on PEN ML/SiO_2. The KPFM result indicates that not a charge transfer but a dipole induced in π orbital of molecules by surface charges determines the VL shift, since the head-to-tail conformation avoids the hybridization between π orbitals.

In Sec. 5-4, I prepared hetero-multilayer of PEN and PFP on SiO_2. There appear the films with various conformations. The origins of the VL shifts at the interfaces with well-defined conformations are simply determined by charge transfer and/or polarization. In addition, it is found that a further deposition is associated with a high possibility of an unexpected mixing. The origin of the VL shift for mixed films is still unclear, since the properties inside is not observed in my measurement.

In Sec. 5-5-2, the KPFM of n-thiophene and PFP hetero-MLs with face-to-face conformation have carried out. 5T, 6T, and 7T in hetero-MLs show an upward VL shift, while PFP shows a downward VL shift. The VL shift of n-thiophene and PFP becomes larger with number of a thiophene ring. These results indicate that charge transfer occurs from lower part of n-thiophene to PFP, since n-thiophene is longer than PFP. The partial charge transfer causes the polarization in n-thiophene, resulting in an upward VL shift. Since the energy difference between HOMO of n-thiophene and LUMO of PFP is larger with ring number, more electrons of n-thiophene move to PFP. As a result, the VL shifts of n-thiophene and PFP increase with molecular length. Thus, I demonstrate the length dependence of the VL shift at D-A interface with a face-to-face conformation.

In Sec. 5-5-4, the head-to-tail hetero-ML of PFP on 6T is also examined. The dipole is induced in π orbital of PFP by surface charge of 6T, such as head-to-tail PEN-PFP hetero-ML. The VL shift of PFP on 6T is larger than that on OH-SiO$_2$, indicating that the charge distribution of both molecules induces a dipole in each π orbital of the films.

Most of PS experiments have so far emphasized a charge transfer caused by the energy level difference between two different materials in the determination of a VL shift at their interface. From the experimental results, IDIS model was established by the introduction of CNLs [11,12,18].

Contrary to this proposal, I focused on the hybridization of the energy level between two different materials. At an O-I interface, the hybridization strongly depends on the thickness of insulating film between an OM and a background conducting material. In the case of a thin insulating film, the energy level alignment between an OM and a background conducting material determines the VL shift on the base of IDIS model. With increase of thickness in insulating films, the electrostatic interaction of organic films with the surface charge of the insulating film becomes a dominant factor owing to weak hybridization.

On the other hand, the displacement of the π orbital in two molecules plays an important role in determining a VL shift at a D-A interface. When the π frame of two molecules is faced each other, the energy difference between the HOMO of donor and the LUMO of acceptor determines a VL shift. In the separation of the π frames, the VL shift at a D-A interface originates not from the energy level alignment but also from the electrostatic interaction with their charge distributions. These results are considered to be similar to the electronic structures of a D-A dimer obtained by theoretical calculations. Thus, I conclude that the structural dependence of the VL shift can be obtained with the preparation of a well-defined conformation and the local measurement by KPFM.

The next step in this ongoing project is to obtain geometric and electrostatic properties at a D-A interface in a single molecular level. The combination of KPFM with NC-AFM gives us a single molecular image, indicating more understanding of the interface properties, such as the propagation of a dipole between neighboring molecules. Another topic of interest is to obtain a direct observation of an intramolecular dipole induced by other material. X-ray specular reflection is a great tool to obtain cross-sectional electron densities according to distance from a substrate [70]. Furthermore, theoretical approaches are essential to verify the applicability of Helmholtz equation to organic films.

Reference

[1] S. R. Forrest, Chem. Rev. **97** (1997) 1793.

[2] H. Ishii, K. Sugiyama, E. Ito, and K. Seki, Adv. Mater. **11** (1999) 605.

[3] D. Cahen and A. Kahn, Adv. Mater. **15** (2003) 271.

[4] N. Koch, Chem. Phys. Chem. **8** (2007) 1438.

[5] N. Koch, A. Vollmer, S. Duhm, Y. Sakamoto, and T. Suzuki: Adv. Mater. **19** (2007) 112.

[6] S. Duhm, G. Heimel, I. Salzmann, H. Glowatzki, R. L. Johnson, A. Vollmer, J. P. Rabe, and N. Koch: Nature Mater. **7** (2008) 326.

[7] S. Braun, W. R. Salaneck, and M. Fahlman: Adv. Mater. **21** (2009) 1450.

[8] V. Heine, Phys. Rev. **138** (1965) A1689.

[9] C. Tejedor, E. Louis and F. Flores, J. Phys. **C 10** 2163 (1977).

[10] W. Mönch, Surf. Sci. **299** (1994) 928.

[11] H. Vázquez, R. Oszwaldowski, P. Pou, J. Ortega, R. Pérez, F. Flores and A. Kahn. Europhys. Lett. **65** (2004) 802.

[12] H. Vázquez, F. Flores, R. Oszwaldowski, J. Ortega, R. Pérez and A. Kahn. Appl. Surf. Sci., **234** (2004) 108.

[13] V. Papaefthimiou, A. Siokou, and S. Kennou, J. Appl. Phys. **91** (2002) 4213.

[14] V. Papaefthimiou, A. Siokou, and S. Kennou, Thin Solid Films **459** (2004) 32.

[15] V. Papaefthimiou, A. Siokou, and S. Kennou, Surf. Sci. **569** (2004) 207.

[16] L. Chen, R. Ludeke, X. Cui, A. G. Schrott, C. R. Kagan, and L. E. Brus: J. Phys. Chem. **B 109** (2005) 1838.

[17] L. Chen, O. Cherniavskaya, A. Shalek, and L. E. Brus, Nano Lett. **5** (2005) 2241.

[18] M. G. Helander, Z. B. Wang, J. Qiu, and Z. H. Lu, Appl. Phys. Lett. **93** (2008) 193310.

[19] K. Puntambekar, J. Dong, G. Haugstad, and C. D. Frisbie: Adv. Funct. Mater. **16** (2006) 879.

[20] S. A. Burke, J. M. LeDue, Y. Miyahara, J. M. Topple, S. Fostner, and P. Grütter: Nanotechnology **20** (2009) 264012.

[21] J. Alexander and S. Magonov, J. Vac. Sci. Technol. **B 27** (2009) 903.

[22] S. C. Veenstra, and H. T. Jonkman, J. Polym. Sci., Part **B**: Polym. Phys., **41** (2003) 2549.

[23] O. V.Molodtsova, T. Schwieger, M. Knupfer, Appl. Surf. Sci., **252** (2005) 143.

[24] Y. Ge, and J. E. Whitten, Chem. Phys. Lett., **448** (2007) 65.

[25] W. Osikowicz, M. P. de Jong, W. R. Salaneck, Adv. Mater. **19** (2007) 4213.

[26] H. Vazquez, F. Flores and A. Kahn, Proc. Int. Symp. Super-Functionality Organic Devices, *IPAP Conf. Series* **6** (2005) 1.

[27] H. Vázquez, F. Flores, and A. Kahn, Org. Electro. **8** (2007) 241.

[28] I. Avilov, V. Geskin, and J. Cornil, Adv. Funct. Mater. **19** (2009) 624.

[29] S. Verlaak, D. Beljonne, D. Cheyns, C. Rolin, M. Linares, F. Castet, J. Cornil, and P. Heremans, Adv. Funct. Mater. **19** (2009) 3809.

[30] M. Linares, D. Beljonne, J. Cornil, K. Lancaster, J-L. Brédas, S. Verlaak, A. Mityashin, P. Heremans, A. Fuchs, C. Lennartz, J. Idé, R. Méreau, P. Aurel, L. Ducasse, and F. Castet, J. Phys. Chem. **C 114** (2010) 3215.

[31] W. Chen, S. Chen, S. Chen, Y-L. Huang, H. Huang, D. C. Qi, X. Y. Gao, J. Ma, and A. T. S. Wee, J. App. Phys. **106** (2009) 064910.

[32] S. Duhm, I. Salzmann, G. Heimel, M. Oehzelt, A. Haase, R. L. Johnson, J. P.

Rabe, and N. Koch, Appl. Phys. Lett. **94** (2009) 033304.

[33] G. Binnig and H. Rohrer. Helv. Phys. Acta, **55** (1982) 726.

[34] G. Binnig, H. Rohrer, C. Gerber, and E. Weibel, Phys. Rev. Lett. **50** (1983) 123.

[35] J. V. Barth, H. Brune, G. Ertl, and R. J. Behm, Phys. Rev. **B 42** (1990) 9307.

[36] D. K. Biegelsen, R. D. Bringans, J. E. Northrup, and L.-E. Swartz, Phys. Rev. **B 41** (1990) 5701.

[37] T. W. Odom, J-L. Huang, P. Kim, and Charles M. Lieber, Nature **391** (1998) 62.

[38] J. Wintterlin, J. Wiechers, H. Brune, T. Gritsch, H. Höfer, and R. J. Behm, Phys. Rev. Lett. **62** (1989) 59.

[39] F. J. Giessibl, Rev. Mod. Phys. **75** (2003) 949.

[40] G. Binnig, C. F. Quate, and C. Gerber, Phys. Rev. Lett. **56** (1986) 930.

[41] Y. Martin, C. C. Williams, and H. K. Wickramasinghe, J. Appl. Phys. **61** (1987) 4723.

[42] T. R. Albrecht, P. Grütter, D. Horne, and D. Rugar. J. Appl. Phys. **69** (1991) 668.

[43] F. J. Giessibl, Science **267** (1995) 1451.

[44] O. Marti, J. Colhero, and J. Mlynek, Nanotechnology **1** (1990) 141.

[45] G. Meyer and N. M. Amer, Appl. Phys. Lett. **57** (1990) 2089.

[46] Y. Martin, D. W. Abraham, P. C. D. Hobbs, and H. K. Wickramasinghe, Electrochemical Sot. Proc. Mug. Mat. Process. Dev. **90** (1989) 115.

[47] P. Griitter, H. J. Mamin and D. Rugar, in Scanning Tunneling Microscopy and Related Techniques R. Wiesendanger and H.-J. Giintherodt, eds., Springer Topics in Surface Science, Springer Verlag, Berlin (1992), p. 151.

[48] C. Schonenberger and S. F. Alvarado, Phys. Rev. **B 80** (1990) 373.

[49] C. C. Williams, Annu. Rev. Mater. Res. **29** (1999) 471.

[50] L. Kantorovich, A. Livshits, and M. Stoneham, J. Phys.: Condens. Matter **12** (2000) 795.

[51] Y. Naitou, A. Ando, H. Ogiso, S. Kamiyama, Y. Nara, and K. Nakamura, Appl. Phys. Lett. **87** (2005) 252908.

[52] Y. Sugimoto, P. Pou, M.Abe, P. Jelinek, R. Pérez, S. Morita**1** and Ó. Custance, Nature **446** (2007) 64.

[53] L. Nony, A. S. Foster, F. Bocquet, and C. Loppacher, Phys. Rev. Lett. **103** (2009) 036802.

[54] L. Gross, Fabian Mohn, P. Liljeroth, J. Repp, F. J. Giessibl, G. Meyer, Science **324** (2009) 1428.

[55] L. Kelvin, Phil. Mag. **46** (1898) 82.

[56] J. M. R. Weaver and D. W. Abraham, J. Vac. Sci. Technol. **B 9** (1991) 1559.

[57] S. Hudlet, M. Saint-Jean, C. Guthmann, and J. Berger, Eur. Phys. J. **B 2** (1998) 5.

[58] U. Zerweck, C. Loppacher, T. Otto, S. Grafström, and L. M. Eng, Nanotechnology **18** (2007) 084006.

[59] F. Bocquet, L. Nony, C. Loppacher, and T. Glatzel, Phys. Rev. **B 78** (2008) 035410.

[60] A. Takagi, F. Yamada, T. Matsumoto, and T. Kawai, Nanotechnology **20** (2009) 365501.

[61] H. Sugimura, and N. Nakagiri, J. Photopolym. Sci. Technol. **10** (1997) 661.

[62] H. Sugimura, K. Hayashi, N. Saito, N. Nakagiri, O. Takai, J. Jpn. Phys. Soc. **188** (2002) 403.

[63] M. Maccarini, M. Himmelhaus, S. Stoycheva, M. Grunze, Appl. Surf. Sci. **252** (2005) 1941.

[64] T. Baldacchini, J. E. Carey, M. Zhou, and E. Mazur, Langumuir **22** (2006) 4917.

[65] T. Yokoyama, C. B. Park, T. Nishimura, K. Kita, and A. Toriumi, J. Jpn. Appl. Phys. **47** (2008) 3643.

[66] N. Koch, Chem. Phys. Chem. **8** (2007) 1438–55.

[67] T. Hasegawa and J. Takeya, Sci. Technol. Adv. Mater. **10** (2009) 024314.

[68] Y. Yamashita, Sci. Technol. Adv. Mater. **10** (2009) 024313.

[69] A. S. Wanl, J. P. Long, G. Kushto, A. J. Mäkinen: Chem. Phys. Lett. **463** (2008) 72.

[70] A. R. Murphy, J. M. J. Frechet, P. Chang, J. Lee, and V. Subramanian, J. Am. Chem. Soc.**126** (2004) 1596.

[71] S. Tatemichi, M. Ichikawa, T. Koyama, and Y. Taniguchi, Appl. Phys. Lett. **89** (2006) 112108.

[72] S. Nagamatsu, K. Kaneto, R. Azumi, M. Matsumoto, Y. Yoshida, and K. Yase, J. Phys. Chem B **109** (2005) 9374.

[73] http://accelrys.com/products/materials-studio/quantum-and-catalysis-software.html

[74] S. E. Fritz, S. M. Martin, C. D. Frisbie, M. D. Ward, and M. F. Toney: J. Am. Chem. Soc. **126** (2004) 4084.

[75] S. D. Wang, X. Dong, C. S. Lee, and S. T. Lee, J. Phys. Chem **B 109** (2005) 9892.

[76] A. Hinderhofer, U. Heinemeyer, A. Gerlach, S. Kowarik, R. M. J. Jacobs, Y. Sakamoto, T. Suzuki, and F. Schreiber: J. Chem. Phys. **127** (2007) 194705.

[77] S. Schiefer, M. Huth, A. Dobrinevski, and B. Nickel: J. Am. Chem. Soc. **129** (2007) 10316.

[78] D. Nabok, P. Puschnig, C. Ambrosch-Draxl, O. Werzer, R. Resel, and D-M. Smilgies: Phys. Rev. **B 76** (2007) 235322.

[79] Y-C. Yeo, T-J. King, and C. Hu: J. Appl. Phys. **92** (2002) 7266.

[80] T. V. Deasai, A. R. Woll, F. Schreiber, and J. R. Engstrom: J. Phys. Chem. **C 114** (2010) 20120.

[81] Y. Inoue, Y. Sakamoto, T. Suzuki, M. Kobayashi, Y. Gao, and S. Tokito, Jpn. J. Appl. Phys. **44** (2005) 3663.

[82] T. N. Krauss, E. Barrena, D. G. de Oteyza, X. N. Zhang, J. Major, V. Dehm, F. Würthner, and H. Dosch, J. Phys. Chem. **C 113** (2009) 4502.

[83] I. Eisenstein, and R. W. Munn, Chem. Phys. **77** (1983) 47.

[84] S. Tatemichi, M. Ichikawa, T. Koyama, and Y. Taniguchi: Appl. Phys. Lett. **89** (2006) 112108.

[85] J. O. Vogel, I. Salzmann, R. Opitz, S. Duhm, B. Nickel, J. P. Rabe, and N. Koch, J. Phys. Chem. **B 111** (2007) 14097.

[86] T. N. Krauss, E. Barrena, D. G. de Oteyza, X. N. Zhang, J. Major, V. Dehm, F. Würthner, and H. Dosch: J. Phys. Chem. **C 113** (2009) 4502.

[87] H. Peisert, M. Knupfer, and J. Fink, Appl. Phys. Rev. **81** (2007) 2400.

[88] S. Duhm, S. Hosoumi, I. Salzmann, A. Gerlach, M. Oehzelt, B. Wedl, T-L. Lee, F. Schreiber, N. Koch, N. Ueno, and S. Kera, Phys Rev. **B 81** (2010) 045418.

[89] Y. Sakamoto, T. Suzuki, M. Kobayashi, Y. Gao, Y. Fukai, Y. Inoue, F. Sato, and S. Tokito, J. Am. Chem. Phys. **126** (2004) 8138.

[90] J.-Z. Wang, J. T. Sadowski, Z.-H. Xiong, Y. Fujikawa, Q. K. Xue, and T.

Sakurai, Nanotechnology **20** (2009) 095704.

[91] A. Hinderhofer, C. Frank, T. Hosokai, A. Resta, A. Gerlach, and F. Schreiber, J. Chem. Phys. **134** (2011) 104702.

[92] R. Ruiz, B. Nickel, N. Koch, L. C. Feldman, R. F. Haglund, A. Kahn, and G. Scoles, Phys. Rev. **B 67** (2003) 125406.

Acknowledgements

I would like to thank my supervisor, Prof. Dr. Hirokazu Tada for providing me with the opportunity to do this doctoral work. His knowledge, ideas and suggestions were very helpful for me. I would like to say that I have benefited a lot under his supervision.

I would also like to thank Prof. Dr. Ken-ichi Fukui and Prof. Dr. Hidekazu Tanaka for accepting to referee this work.

I would like to express my gratitude to Associate Prof. Dr. Ryo Yamada. To a great extent, his scientific motivation kept my thesis running. I wish to thank for his guidance, support, and encouragement.

I am very grateful to Dr. Yoshitaka Kawasugi and Dr. Masato Ara for having lunchbreaks with interesting scientific and non-scientific discussions.

I would also like to express my thanks to my fellow colleagues in the group, especially Lee See Kei, Ngyuen Thu Loan, Koji Takahashi, Junichi Nakagawa, and Gu Heng for assistance in my research.

Finally, I want to thank my family. Their continuous support and love during this thesis was really appreciated.

Publication List

Papers

1. Ryota Mishima, Ngyuen Thu Loan, and Hirokazu Tada, 「Electrostatic Properties of Organic Monolayers on Silicon Oxides Studied by Kelvin Probe Force Microscopy」, 『Jpn. J. Appl. Phys.』 accepted.
2. Ryota Mishima, Masaki Takada and Hirokazu Tada, 「STM Studies of NaCl Thin Films on Cu(111) Surface at Low Temperature」, 『Mol. Cryst. Liq. Cryst.』 472, 321-325 (2007).

Oral Presentations

Domestic Conferences

1. 三島良太、高田正基、Wilson Agerico Dino、夛田博一、赤井久純、「Au(111)表面上における Mn 合金の低温走査トンネル分光測定」、『日本物理学会 2009 春季大会』、東京、2009 年 3 月
2. 三島良太、中川純一、夛田博一「Au(111)表面上のフタロシアニン単分子膜のバリアハイト測定」、『応用物理学会 2009 秋季大会』、富山、2009 年 9 月
3. 三島良太, Gayani Perera, Saw-Wai Hla, 夛田博一「Au(111)表面上のドナーおよびアクセプタ分子の dI/dV 分光測定」『応用物理学会 2010 年秋季大会』、長崎、2010 年 9 月

International Conferences

1. Ryota Mishima, Masaki Takada, Hirokazu Tada, 「Scanning tunneling microscopy and spectroscopy of Mn alloys on Au(111)」, 『NSS5-SPSTM2』, Ohio, USA (July 2008)

2. Ryota Mishima, 「Electrostatic Properties of Organic Films Studied by Kelvin Probe Force Microscopy」 『International Conference on Core Research and Engineering Science of Advanced Materials』, Osaka, Japan (June 2010)
3. Ryota Mishima, and Hirokazu Tada, 「Electrostatic Properties of Organic Films on Silicon Oxides Studied by Kelvin Probe Force Microscopy」, 『SSSJ-A3 Foresight Joint Symposium on Nanomaterials and Nanostructures』, Tokyo, Japan (July 2010)

6 Poster Presentations